The adhesion GPCR Adgrd1 is a prion protein receptor and a mediator of prion cytotoxicity

Asvin KK Lakkaraju[1#], Oliver Tejero[2#], Ramon Guixà-González[3,4], Elena De Cecco[1], Martina Jungo[1], Ching-Ju Tsai[2], Rocco Mastromartino[1], Jacopo Marino[2], Xavier Deupi[2,3,4], Simone Hornemann[1], Gebhard FX Schertler[2], and Adriano Aguzzi[1]*

[1] Institute of Neuropathology, University of Zurich, Schmelzbergstrasse 12, 8091 Zurich, Switzerland.

[2] Laboratory of Biomolecular Research, Division of Biology and Chemistry, Paul Scherrer Institute, Forschungsstrasse 111, 5232 Villigen PSI, Switzerland.

[3] Condensed Matter Theory Group, Laboratory for Theoretical and Computational Physics, Division of Scientific Computing, Theory and Data, Paul Scherrer Institute, Forschungsstrasse 111, 5232 Villigen PSI, Switzerland.

[4] Swiss Institute of Bioinformatics (SIB), Quartier Sorge - Batiment Amphipole, 1015 Lausanne, Switzerland.

[#] equal contribution

Correspondence to: Adriano Aguzzi
Institute of Neuropathology, University Hospital of Zürich
Schmelzbergstrasse 12
CH-8091 Zürich, Switzerland
Phone: +41 (1) 255-2107, FAX: +41 (1) 255-4402
E-mail: adriano.aguzzi@usz.ch

Abstract

In prion diseases, the cellular prion protein PrP^{C} is converted into aggregates of PrP^{Sc}, leading to profound neurotoxicity through largely unknown mechanisms. Here we report that the cellular prion protein PrP^{C} acts as an antagonist of the adhesion G protein-coupled receptor (GPCR) Adgrd1. When overexpressed in cultured cells, Adgrd1 recruited the G-protein Gαs, inducing excessive cytosolic cAMP, growth arrest and cytotoxicity, all of which were suppressed by $FT_{25\text{-}50}$, a 26-meric peptide from the N-terminal flexible tail (FT) of PrP^{C}. We found that $FT_{25\text{-}50}$ forms a complex with Adgrd1 and suppresses its intrinsic activation by the Stachel peptide. Adgrd1 ablation attenuated the neurodegeneration of prion-infected cerebellar organotypic slice cultures and prolonged the healthspan of prion-infected mice. Interaction studies with mutated proteins, computational modeling and docking studies revealed that suppression of Adgrd1 signaling requires the polybasic domain of the FT and the N-terminal fragment of Adgrd1. In the absence of PrP^{C}, the cAMP spike caused by Adgrd1 was suppressed by co-expression of a functionally dead Adgrd1-Adgrg6 chimeric receptor, suggesting that Adgrd1 activation requires an unidentified agonistic ligand displaced by $FT_{25\text{-}50}$. These results identify Adgrd1 as a mediator of prion toxicity and suggest that Adgrd1 modulators may be beneficial against prion-related neurodegeneration.

Introduction

In prion diseases, the endogenous cellular prion protein (PrP^{C}), a GPI-anchored extracellular protein, is converted into misfolded, aggregated conformers termed PrP^{Sc} (Prusiner, 1982). Cell-surface expression of PrP^{C} is essential not only for its conversion into infectious prions (Bueler *et al*, 1993), but also for mediating their neurotoxicity (Brandner *et al*, 1996). PrP^{C} is enriched in lipid rafts, where it can interact with several membrane proteins. The transition of PrP^{C} to PrP^{Sc} and its associated conformational changes may impair these interactions and contribute to neurotoxicity in prion diseases.

PrP^{C} interacts with multiple families of G protein-coupled receptors (GPCRs) through its flexible N-terminal tail (FT). The interaction of FT with the adhesion GPCR Adgrg6 promotes myelination in the peripheral nervous system (Kuffer *et al*, 2016). Furthermore, PrP^{C} interacts with the metabotropic glutamate receptors mGluR1 and mGluR5 (Um *et al*, 2013). Drugs targeting mGluR1/5 reduce the neurodegeneration observed in prion-infected cerebellar slice cultures and delay disease onset in prion-infected mice (Goniotaki *et al*, 2017). Adgrd1 belongs to group V of the adhesion GPCR family. It is upregulated in glioblastoma, a malignant astrocytic tumor of humans (Bayin *et al*, 2016), and its downregulation reduces the growth of glioblastoma in mice (Frenster *et al*, 2020). Many single-nucleotide polymorphisms were reported in the Adgrd1 gene, some of which affect its surface expression and signaling activity (Fischer *et al*, 2016). Adgrd1 contains a pentraxin (PTX) domain followed by the conserved GPCR autoproteolysis-inducing (GAIN) domain and by the seven-transmembrane domain (7TM). During its biosynthesis, Adgrd1 is proteolytically cleaved at the GPCR proteolysis site (GPS) within the GAIN domain, resulting in an N-terminal fragment (NTF) and a C-terminal fragment (CTF) [10]. The NTF and the CTF remain non-covalently attached and reside in the plasma membrane. NTF dissociation may occur through interactions with extracellular stimuli and allows binding of the tethered agonist peptide to the 7TM, leading to the activation of the receptor, recruiting and activation of Gs proteins, and production of cAMP.

Here we report that binding of the N-terminus of the prion protein to activated Adgrd1 can suppress its activity and prevent Gs-mediated signaling and intracellular cAMP spikes. Furthermore, genetic ablation of Adgrd1 protected cerebellar organotypic cultured slices (COCS) from prion induced toxicity and improved the health span, though not the life span, of mice infected with prions.

Results

FT suppresses Adgrd1 mediated signaling

A 28-meric peptide corresponding to the N-terminus of the flexible tail of the cellular prion protein PrP^C (termed FT_{23-50}) can act as an agonist of the adhesion GPCR Adgrg6 (Kuffer *et al.*, 2016). As PrP^C is known to interact with several GCPRs (Goniotaki *et al.*, 2017; Khosravani *et al*, 2008; Peggion *et al*, 2011; Senatore *et al*, 2012), we asked if the activity of further adhesion GPCRs may be modulated by FT. We transiently expressed full-length Adgra2, Gpr176, Adgrg1, Adgrg3, Adgrg2, Adgrg6 and Adgrd1 in HEK293T cells, and exposed them to FT_{23-50}. Expression of Adgrd1, but not of any other tested GCPR, led to a 7-fold increase of intracellular cAMP that was almost completely prevented by administration of FT_{23--50} (**Fig. 1A**). This suggests that Adgrd1 is either constitutively active in HEK293T cells, or is activated by an unknown ligand, and that

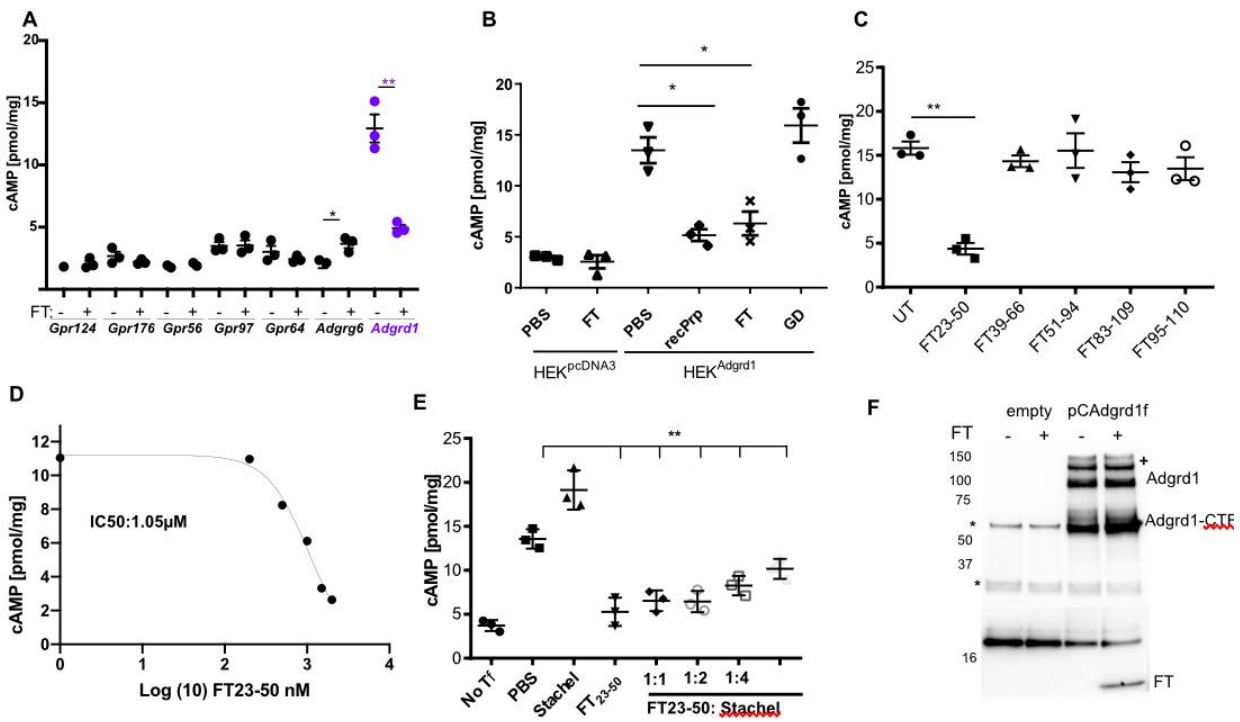

Figure 1: FT is an antagonist of Adgrd1 signaling. **A**: HEK293T cells were transiently transfected with Gpr124, Gpr176, Gpr56, Gpr97, Gpr64, Adgrg6, Adgrd1 and 24hours later were incubated with either FT_{23-50} (2µM; 20 min) or as control with PBS. FT_{23-50} treatment resulted in a cAMP spike in Adgrg6 transfected cells and reduced the cAMP levels in Adgrd1 transfected cells. FT_{23-50} treatment did not induce any cAMP changes in other transfected cells. cAMP levels were measured using ELISA. Unpaired t-test. Each dot represents data obtained from an individual experimental replicate. **B:** HEK293T cells were transiently transfected with empty plasmid (pCDNA3) or with human Adgrd1-expressing plasmid. After 48h, cells were treated with PBS, full-length recombinant PrP (recPrP), (5 mg/ml) recombinant FT (residues. 23-110; 5 µM) or the recombinant globular domain of PrP (GD; 5 µM). After 30 min intracellular cAMP was measured using an immunoassay. Adgrd1 expression caused a large cAMP spike, which was quenched by recPrP and FT, but not by GD or PBS. Unpaired t-test. **C:** HEK293T cells transfected with a plasmid expressing human Adgrd1 for 48h were exposed to FT derived peptides (2 µM; 30 min). Only FT_{23-50} abrogated the cAMP response. Unpaired t-test. **D:** HEK293T cells expressing Adgrd1 were exposed to FT_{23-50} (0-5 µM; 30 min). Intracellular cAMP was measured, and a dose response curve was generated. Increasing amounts of FT_{23-50} dose-dependently suppressed Adgrd1 signaling. Unpaired t-test. **E:** HEK293T cells expressing Adgrd1 were exposed to FT_{23-50}, Stachel or a combination of FT_{23-50} + Stachel at different molar ratios (2 µM:100 µM (1:1); 2 µM:200 µM (1:2); 2 µM:400 µM (1:4); 2 µM:800 µM (1:8)) for 30 min. Exposure to Stachel alone increased cAMP levels while FT_{23-50} treatment abolished the cAMP response. Mix of FT_{23-50} and Stachel also reduced the cAMP response despite increasing concentrations of the Stachel peptide. These results suggest that in the presence of FT, the Stachel peptide cannot exert its agonistic activity. Unpaired t-test. **F:** HEK293T cells expressing Adgrd1 with a C-terminal Flag epitope exposed to recombinant FT_{23-110} (2 µM; 30 min) and subjected to immunoprecipitation using an anti-Flag antibody, followed by western blotting with POM2 or anti-Flag antibody. Anti-Flag antibody detected full length Adgrd1 protein and cleaved CTF of Adgrd1. POM2 revealed a band corresponding to FT that co-precipitated with Adgrd1. Asterisk: Immunoglobulin heavy and light chains. +: oligomers of Adgrd1.

FT_{23-50} acts as its antagonist or inverse agonist. As reported previously, FT_{23-50} increased cAMP levels in Adgrg6-expressing cells, yet it did not modulate cAMP in cells transfected with any of the other tested GPCRs (**Fig. 1A**). To confirm that this modulation is specific to PrP, we treated HEK293T cells transiently transfected with Adgrd1 (henceforth called HEK^{Adgrd1}) with bacterially expressed full-length human prion protein (23-231 aa), FT (23-110 aa), or globular domain (GD; 121-231 aa) of PrP. Treatment with recombinant PrP or FT, but not with GD, prevented the cAMP spike in HEK^{Adgrd1} cells (**Fig. 1B**).

Next, we sought to delineate the minimal FT domain responsible for Adgrd1 antagonism. HEK^{Adgrd1} cells were exposed to a series of overlapping peptides covering residues 23-110 of PrP. Only a peptide spanning residues 23-50 suppressed Adgrd1 activation (**Fig. 1C**). Exposure of HEK^{Adgrd1} cells for 30 min to increasing concentration of FT_{23-50} resulted in progressive cAMP reduction with an IC_{50} of 1.05 µMol (**Fig. 1D**).

We next asked if the FT_{23-50} mediated suppression of Adgrd1 can be relieved by the Stachel peptide which activates Adgrd1 (Liebscher *et al*, 2015). Treatment of HEK^{Adgrd1} cells with Stachel (100 µM; 30 min) resulted in a cAMP surge, which was suppressed when cells were simultaneously treated with FT_{23-50} and Stachel. Suppression could not be overridden by increasing the Stachel concentration (**Fig. 1E**). Hence, binding of FT_{23-50} prevents, directly or indirectly, Stachel-mediated overactivation of Adgrd1. We therefore asked if there is a physical interaction between FT_{23-50} and Adgrd1. Indeed, FT_{23-50} co-precipitated with Adgrd1 in HEK^{Adgrd1} cells, but not in untransfected HEK cells (**Fig. 1F**). This suggests that Adgrd1 can form a complex with FT_{23-50}.

Defining the interaction domains of FT and Adgrd1

We next sought to characterize the interaction domains on the FT and Adgrd1 that are involved in cAMP regulation. We hypothesized that the polycationic domain KKRPK, which is critical in modulating Adgrg6 activity, might also be involved in suppressing Adgrd1 activity. A phylogenetic analysis showed that the basic residues within the KKRPK domain are perfectly conserved among 141 mammalian species (**Fig. 2A**) suggesting that this motif serves important physiological functions. We therefore treated HEK^{Adgrd1} cells with a polyalanine mutant of the FT_{23-50} peptide (KKRPKPG → AAAPAPG) **(Fig. 2A)**. Treatment of HEK^{Adgrd1} cells with wild-type FT_{23-50} (2 µM, 30 min) reduced cAMP levels whereas the mutant peptide had no effect (**Fig. 2B**). Sequence alignments had previously shown two regions of similarity between FT and collagen IV (KKRPK and QGSPG), an agonistic ligand of Agrg6. We investigated if the presence of the QGSPG sequence in $FT_{23.-50}$ is required for suppressing Adgrd1-mediated cAMP enhancement. A FT_{23-50} peptide containing a mutated QGSPG sequence suppressed the cAMP spike, similarly to native FT_{23-50-} (**Fig. 2B**). Hence, it is the cationic domain of FT_{23-50} which is essential for its antagonistic activity on Adgrd1. We then generated two smaller peptides: FT_{23-35} and FT_{25-37}. Both peptides abrogated the induction of cAMP in HEK^{Adgrd1} cells, indicating that the distal three residues (RPK) of the KKRPK domain are crucial region for the suppression of Adgrd1 activity (**Fig. 2C**).

The modulation of Adgrd1 activity may rely on the charge imparted by cationic residues onto FT_{23--50}, rather than the identity of the residues. To test this hypothesis, we mutated all lysines within the KKRPKPG domain into arginines, thereby retaining the positive charges. Treatment of HEK^{Adgrd1} cells with the KKRPKPG → RRRPRPG peptide reduced cAMP similarly to the wild-type peptide (**Fig. 2D**), indicating that the positive charges are essential for Adgrd1 antagonism.

To define the FT-interacting domain on Adgrd1, we generated mutants of human Adgrd1 lacking either the GAIN domain, the PTX domain, or the entire N-terminal extracellular domain beyond the Stachel sequence (**Fig. 2E)**. Full-length and mutant expression plasmids were transfected in HEK293T cells and treated with FT_{23-50} (2 µM; 30 min). The GAIN domain mutant lacking the Stachel domain did not modulate cAMP with or without FT_{23-50}, indicating that it was non-functional. In contrast, cells expressing the PTX-deleted Adgrd1 mutant showed increased basal cAMP, albeit to a lesser extent than wild-type Adgrd1. This result confirms that Adgrd1 activation requires the GAIN domain. In cells expressing the PTX-deleted mutant, treatment with FT_{23-50} did not block the cAMP increase, suggesting that the presence of PTX domain is essential for FT_{23-50} interaction with Adgrd1. Finally, the mutant lacking the N-terminus caused enhanced cAMP levels which were not suppressed by FT_{23-50} (**Fig. 2F**).

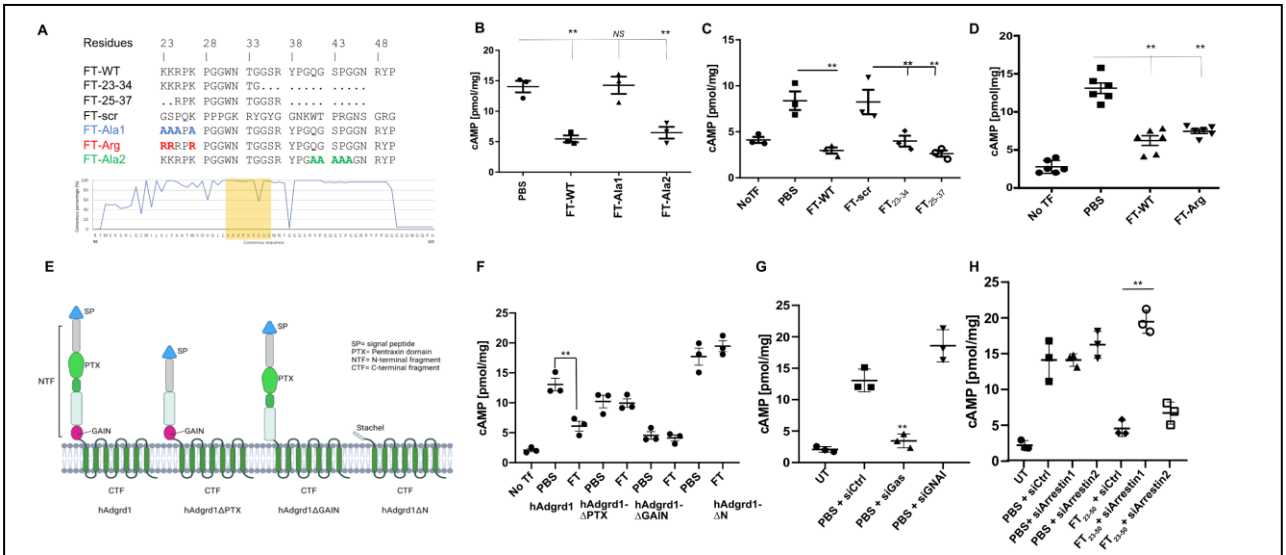

Figure 2: Modulation of Adgrd1 signaling by FT. **A:** Peptides used in panels B-D (upper) and high conservation of the polycationic domain among 141 mammalian species. **B:** Adgrd1-expressing HEK293T cells were exposed to FT_{23-50} peptides (2 µM, 30 min). Alanine replacement of lysines within the KKRP domain abolished cAMP induction by Adgrd1. Replacement of QGSPG in FT_{23-50} did not alter cAMP responses. Unpaired t-test. **C:** HEK293T cells transiently transfected (48 h) with Adgrd1 were exposed to FT-derived peptides (2 µM; 30 min). FT_{23-35} and FT_{25-37} reduced the cAMP spike induced by Adgrd1. Scrambled FT_{23-50} (sFT) was used as a control. Unpaired t-test. **D:** Adgrd1 expressing HEK293T cells were treated with FT_{23-50} peptides bearing arginine substitutions of all lysines (K) in the KKRPKPG domain (2 µM; 30 min). Arginine-substitutions within the KKRPKG motif did not impair cAMP suppression, suggesting positive charges are essential for Adgrd1 modulation. Unpaired t-test. **E:** Adgrg1 deletion mutants utilized in panels F-H. **F:** HEK293T cells were transfected with plasmids encoding human Adgrd1 or mutants lacking the PTX, GAIN or N-terminal domains. 48 h post transfection, cells were exposed to PBS or FT_{23-50} (2 µM; 30 min). FT_{23-50} suppressed cAMP levels in cells expressing wild-type Adgrd1 but in none of the mutants. GAIN domain removal resulted in an inactive receptor, while truncation of entire N-terminus resulted in a constitutively active receptor inducing extensive cAMP increase. Untransfected cells were used to determine the basal cAMP levels in HEK293T cells. Unpaired t-test. **G:** Comparison between non-transfected (UT) and Adgrd1-expressing HEK293T cells transfected with non-targeting siRNA or siRNA targeting the Gαs or Gai genes. Downregulation of Gαs, but not Gai, suppressed the Adgrd1-induced cAMP spike. Unpaired t-test. **H:** HEK293T cells, untransfected (UT) or co-transfected with Adgrd1, were subjected to non-targeting siRNA or siRNA against arrestin 1 and 2. Arrestin downregulation did not alter the cAMP induction by Adgrd1. However, arrestin 1 downregulation prevented the effect of FT_{23-50} on the Adgrd1-induced cAMP response. Downregulation of arrestin 2 did not alter the modulation of Adgrd1 activity by FT_{23-50}. Unpaired t-test.

To further characterize the interaction between FT_{23-50} and the N-terminus of Adgrd1, we predicted the three-dimensional structure of the complex using AlphaFold Multimer (Richard *et al*, 2022). The resulting models suggested that FT_{23-50} interacts with both the GAIN and the PTX domains through its cationic motif KKRPK **(Fig. 3A)**. To assess the plausibility of this interaction, we performed computational docking calculations using a flexible protein–peptide technique. These results also suggest that binding of FT_{23-50} to both the GAIN and PTX domains though its cationic motif is one of the most feasible solutions. The analysis of the electrostatic potential of this complex shows that two separate anionic patches in each of the N-terminal domains of Adgrd1 could mediate this interaction mode with FT_{23-50} **(Fig. 3B)**. These computational findings are congruent with our experimental data showing that both the PTX and the GAIN domains are required for the inhibitory action of FT_{23-50}.

To investigate the type of G protein involved in this signaling module, we used RNAi to suppress the Gα proteins Gαs or Gαi in HEK^{Adgrd1} cells. Downregulation of Gαs, but not of Gαi, prevented the cAMP increase, indicating that activated Adgrd1 signals via the Gαs subunit **(Fig. 2G)**. Arrestins are key in shutting down activated GPCRs. We hypothesized that the interaction with FT_{23-50} might rapidly recruit arrestins, thereby

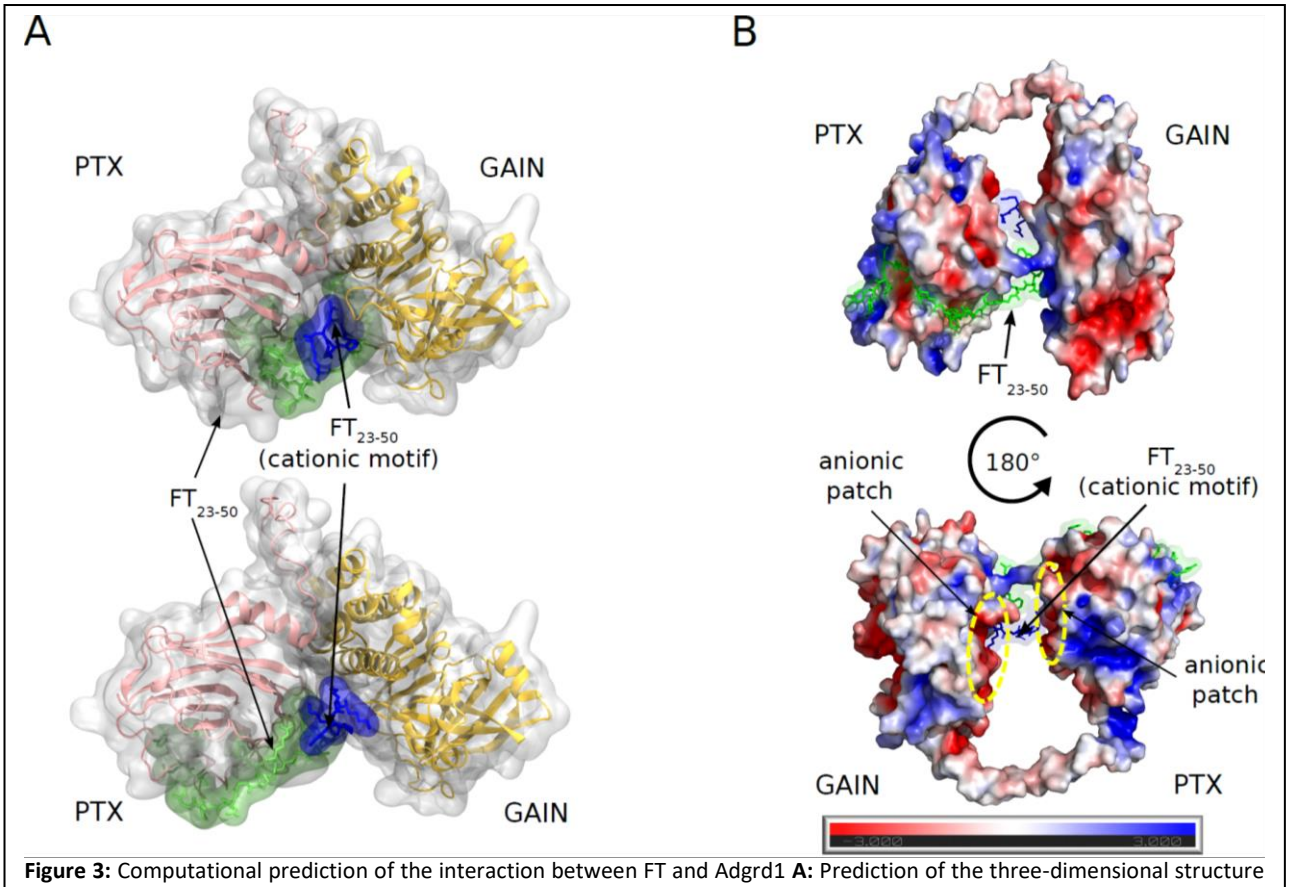

Figure 3: Computational prediction of the interaction between FT and Adgrd1 **A:** Prediction of the three-dimensional structure of the Adgr1 N-terminal domain in complex with FT_{23-50}. Two different representative predictions from AlphaFold Multimer indicate that the Adgr1 N-terminus and FT_{23-50} potentially fold by accommodating the cationic motif of FT_{23-50}, depicted in blue, between the PTX and the GAIN domains, represented in pink and orange cartoons, respectively. **B:** Molecular docking of FT_{23-50} to the N-terminus of Adgrd1. Electrostatic surface potential of FT_{23-50} bound to the N-terminal domain of Adgrd1. Thhe surface representation of a representative binding pose, obtained by flexible protein-peptide docking, and colored by its electrostatic surface potential, shows that two negatively charged regions of the PTX and GAIN domains (circled in yellow) could facilitate the binding of the positively charged portion of FT_{23-50} between both domains.

reducing the cAMP response. To assess this, we used the PRESTO-Tango luciferase-based assay (Kroeze *et al*, 2015). HTLA cells stably expressing arrestin tagged with TEV protease, were transfected with Adgrd1 cDNA bearing a TEV cleavage site and a transcriptional activation domain that drives luciferase expression. Recruitment of arrestins to the receptor results in the cleavage of the transcriptional activator, which in turn translocates to the nucleus and promotes luciferase transcription. Treatment with $FT_{23\text{-}50}$ of $HTLA^{Adgrd1}$ cells resulted in an enhanced luciferase signal, suggesting that arrestins are recruited upon $FT_{23\text{-}50}$ treatment (**Fig. S1B**). To further examine the type of arrestin recruited, RNAi was used to downregulate the expression of arrestin-1 or 2 in HEK^{Adgrd1} cells. Suppression of arrestins did not have any effect on the cAMP levels in PBS-treated cells, while suppression of arrestin-1, but not of arrestin-2, resulted in increased cAMP in cells treated with $FT_{23\text{-}50}$ (**Fig. 2F**). This suggests that $FT_{23\text{-}50}$ binding leads to the recruitment of arrestin 1 to arrest Adgrd1-mediated signaling through the Gαs pathway.

Finally, we investigated if collagen and laminin-211, which have been reported to be agonistic ligands of Adgrg6, can modulate the activity of Adgrd1. HEK^{Adgrd1} cells were treated with either $FT_{23\text{-}50}$ (2 µM; 30 min) or Collagen IV (5 µg/ml; 30 min) or laminin-211 (5 µg/ml; 30 min). While $FT_{23\text{-}50}$ blocked the cAMP increase induced by Adgrd1, collagen IV and laminin-211 did not show such effects (**Fig. S1C**).

The structure of Adgrd1 coupled to Gs

Can the interaction of Adgrd1 and Gs protein be reproduced in vitro with purified components? Plasmids containing full-length Adgrd1 and $Adgrd1^{CTF}$ were designed for expression in High Five insect cells (*Trichoplusia ni*) using the flashBAC™ system (**Fig. S2A**). In parallel, a plasmid for expression of the Gs heterotrimer was designed where the Gαs subunit is fused to the green fluorescent protein (GFP) at the N-terminus. To increase the yield of the Gαs subunit, we used a shortened version of the Gαs subunit (mini-Gαs) in which the flexible α-helical domain was removed and the Ras domain was mutated (G49D, E50N, A249D, S252D, I372A, V375I) to increase the stability of the construct (Carpenter & Tate, 2016).

Firstly, we tested if additional Stachel peptide was needed to trigger G protein binding to the full-length Adgrd1 or the $Adgrd1^{CTF}$. For this purpose, we conducted fluorescence size-exclusion chromatography experiments to analyze Gαs binding with and without the chemically synthesized Stachel peptide (derived from the wild-type Stachel sequence) (Liebscher *et al.*, 2015). For both the full-length Adgrd1 and the $Adgrd1^{CTF}$, addition of the Stachel peptide was necessary to form a complex that is stable enough to survive the SEC purification (**Fig. S2B**).

To obtain the Adgrd1/mini-Gs complex for cryo-electron microscopic (cryo-EM) studies, we used $Adgrd1^{CTF}$ because of its higher expression levels compared to the full-length Adgrd1. The receptor and the G protein heterotrimer were co-transfected in High Five insect cells for 48h. The transfected cells were first incubated with additional Stachel peptide to form the complex followed by cell lysis in the detergent/lipid mixture lauryl

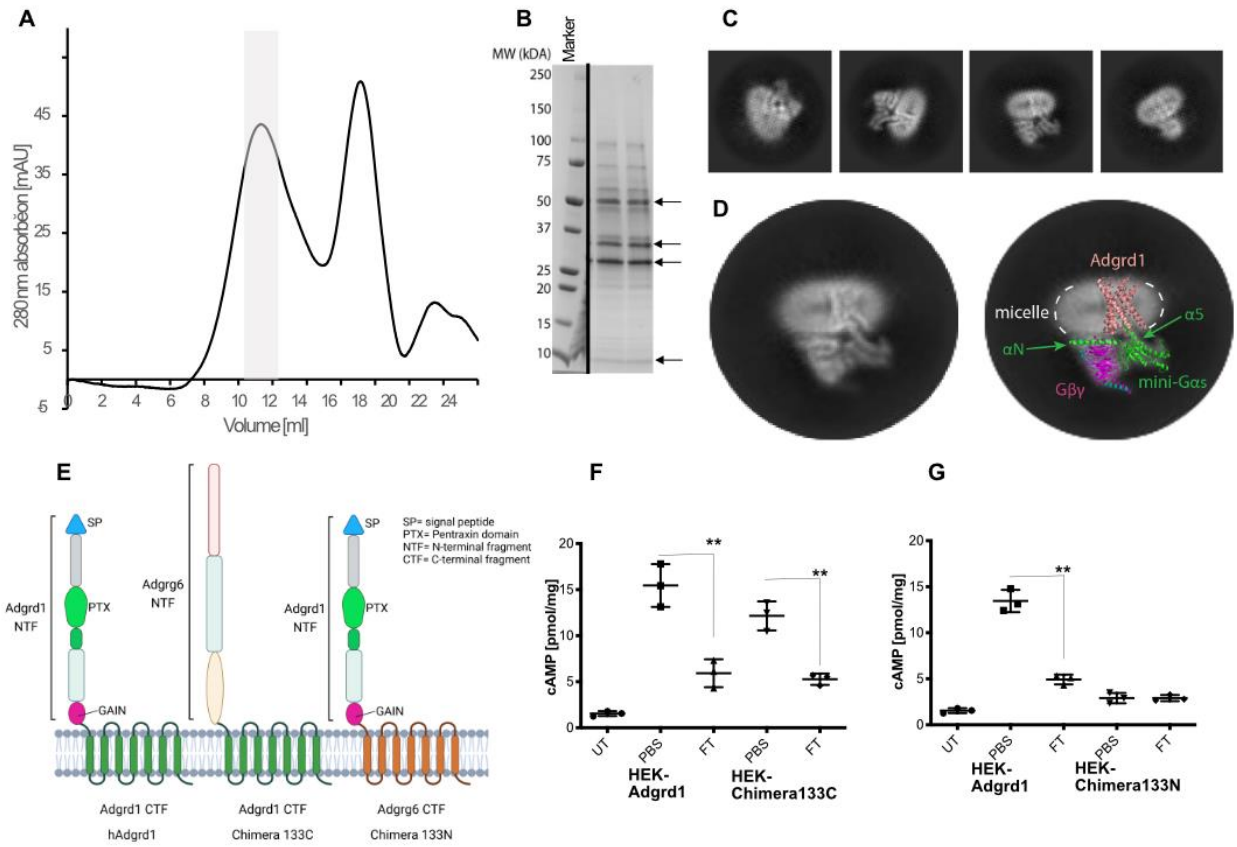

Figure 4: Purification and cryo-EM 2D class average of the Adgrd1-mini-Gs complex. A: SEC elution profile of the Adgrd1^{CTF}/mini-Gs complex purified from an anti-FLAG affinity column. Fractions highlighted in grey were collected for cryo-EM studies. **B:** Coomassie-blue stained SDS-PAGE of the SEC elution fractions used for cryo-EM studies. The theoretical molecular weight of GFP tagged mini-Gs, Gβ, Adgrd1^{CTF} and Gγ are 58 kDa, 39 kDa, 37 kDa and 8 kDa, respectively. **C:** Representative 2D class averages showing the Adgrd1-Gs complex in different orientations. **D:** 2D class average overlaid with the cryo-EM structure of Adgrd1^{CTF}/mini-Gs complex (7EPT.pdb) with complex components labeled (right). The overlaid model shows the Adgrd1 in salmon red, mini-Gαs in green, Gβ in magenta and Gγ in cyan. **E.** Schematic representation of chimeric receptors used in panels F-G. **F:** HEK293T cells were transfected with plasmids containing cDNA of either Adgrd1 or Chimera 133C. 24h post transfection cells were treated with either FT (2µM; 20min) or PBS and intracellular cAMP levels were measured. Both Adgrd1 and Chimera 133 were constitutively active suggesting that C-terminus of Adgrd1 is essential for its constitutive activation. Treatment with FT blocked cAMP responses in both Adgrd1 and Chimera 133C expressing cells suggesting that FT binding prevents C-terminus mediated cAMP accumulation. Unpaired t-test. **G:** HEK293T cells were transfected with plasmids containing cDNA of either Adgrd1 or Chimera 133N. 24h post transfection cells were treated with either FT (2µM; 20min) or PBS and intracellular cAMP levels were measured. Chimera 133N, unliked full length Adgrd1 failed to induce cAMP accumulation emphasizing the crucial role of C-terminus in the cAMP response. FT treatment blocked the induction of Adgrd1 but not alter the endogenous cAMP levels in cells expressing Chimera 133N. Unpaired t-test.

maltose neopentyl glycol/cholesteryl hemisuccinate (LMNG/CHS). The Adgrd1^{CTF}/mini-Gs complex was purified from cell lysate by affinity purification and SEC steps (**Fig. 4AB**, **Fig. S2C**), following plunge freezing for preparation of cryo-EM grids.

The 2D class averages show projections of the complex in different orientations (**Fig. 4C**). To interpret the projection density with the protein components, we docked the available structural model of the Adgrd1^{CTF}/mini-Gs complex into the representative 2D class average (7EPT.pdb) (Ping *et al*, 2022) (**Fig. 4D**). An elongated density, corresponding to the C-terminal α5 helix, extends from mini-Gαs and intrudes into the

Adgrd1^{CTF} cytoplasmic side. This indicates that the Adgrd1^{CTF} is in an active conformation in which the cytoplasmic G protein binding site is formed. The αN helix of mini-Gαs lies along the micelle surface next to the Gβγ subunits. Overall, our 2D class averages agree with the known architecture of active GPCR-G protein signaling complexes.

Domain swapping between Adgrg6 and Adgrd1 suggests the existence of an agonistic Adgrd1 ligand

We next investigated the role of the transmembrane and cytoplasmic domains of Adgrd1 in signaling. We generated chimeric receptors in which Adgrd1^{NTF} was mounted onto Adgrg6^{CTF} (Chimera 133N: Adgrd1^{NTF}-Adgrg6^{CTF}), which is activated agonistically by the FT, and a second chimeric receptor by combining the Adgrg6^{NTF} with theAdgrd1^{CTF} (Chimera 133C: Adgrg6^{NTF}-Adgrd1^{CTF}) (**Fig. 4E**). When expressed in HEK cells, Chimera 133C behaved like Adgrd1 and induced a cAMP response, suggesting that the C-terminal fragment of the protein is critical for constitutive activation and downstream signaling events. Upon FT treatment, the cAMP response was reduced, suggesting that FT prevents the function of C-terminus presumably by preventing conformational changes in the receptor (**Fig. 4F**). Chimera 133N, however, did not result in increased cAMP, suggesting that the presumed endogenous ligand of Adgrd1 does not bind to the N-terminus but acts directly on the C- terminus of the protein and is not reactive to the addition of FT (**Fig. 4G**).

HEK cells were co-transfected with Adgrd1 and increasing amounts of Chimera 133N cDNA. Intracellular cAMP levels revealed that increasing amounts of Chimera133N results in suppressing the cAMP response, suggesting that it acted as a non-functional receptor (Fig.S1C). This suggests that Chimera 133N can actively compete for a hypothetical endogenous Adgrd1 ligand distinct from FT.

Constitutive expression of Adgrd1 is cytotoxic

We expressed Adgrd1 in the human LN229 glioma cell line under doxycycline-dependent (tetOn) transcriptional control (Baron & Bujard, 2000). Induction of Adgrd1 resulted in increased c AMP levels (**Fig. S1D**) and slower growth of cells followed by cell death after 6 days (**Fig. 5A, Movie S1A-B**). To test if cell death is a direct consequence of Adgrd1 activity, we subjected HEK^{Adgrd1} cells to siRNA against the Gαs subunit. Down-regulation of Gαs in HEK^{Adgrd1} cells 5 days post transfection resulted in attenuation of growth impairment ($p<0.001$) (**Fig. 5B**). We next investigated if the Adgrd1-induced cytotoxicity can be rescued by treating the cells with FT_{23-50}. LN229 cells expressing Adgrd1 and treated with doxycycline and FT_{23-50} (5 µM; added every 12 hours) for 6 days exhibited significant improvement in cell viability ($p=0.003$) compared to cells treated with doxycycline and PBS or untreated cells (**Fig. 5C**).

Western blot analysis of lysates from organs of 4-month-old mice revealed the presence of Adgrd1 in the cortex and cerebellum of brains (**Fig. S1E**). This is congruent with single-cell RNA sequencing (Yao *et al*, 2021) showing expression of Adgrd1 in neuronal subsets of mouse brains (**Fig. S1F**).

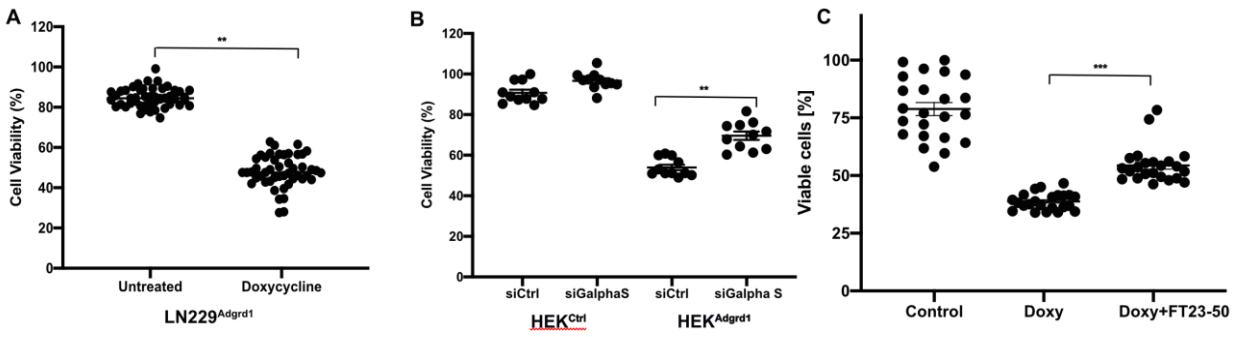

Figure 5: Excessive Adgrd1 signaling is cytotoxic **A:** LN229^{Adgrd1} cells were treated with doxycycline (2 µg/ml) to induce Adgrd1 expression. 6 days post transfection, cell viability was measured with CellTiterGlo. For control, LN229^{Adgrd1} cells were not treated with doxycycline. Each dot represents the cell viability in an individual well of a 96 well plate. Unpaired t-test. **B:** HEK293T cells were transiently transfected with a control plasmid (pCDNA3; HEK^{Ctrl}) or with a plasmid encoding human Adgrd1 (HEK^{Adgrd1}). Cells were then transfected with control siRNA or siRNA against Gαs protein subunits. 5 days post transfection, cell viability was measured using cell counter. Downregulation of Gαs in HEK^{Adgrd1} cells prevented the toxicity induced by Adgrd1. siRNA against Gαs did not induce cellular toxicity in HEK^{Ctrl} cells. Unpaired t-test. **C:** LN229^{Adgrd1} cells were treated with doxycycline (2 µg/ml) to induce Adgrd1 expression, and simultaneously incubated with FT_{23-50} or with PBS. Fresh medium containing doxycycline and FT_{23-50} was added every 12 hours for 6 days. On day 6, cell viability was measured by incubating the live cells with CellTiterGlo. LN229^{Adgrd1} cells that were not stimulated with doxycycline were used as control. Each dot represents viability levels in an individual well of a 96 well plate. Statistics: Unpaired t-test.

Prion diseases are accelerated by PrP^C overexpression (Fischer *et al*, 1996) and prevented by its ablation (Bueler *et al.*, 1993), suggesting a toxic gain-of-function. We hypothesized that signaling of Adgrd1 under physiological conditions is regulated by PrP^C, while in prion diseases the sequestration of PrP^C might upregulate Adgrd1 signaling and contribute to toxicity. To test this hypothesis, we monitored the expression of Adgrd1 in brain lysates of prion-infected mice. At the terminal stage both the RNA (**Fig. S3A**) and protein levels of Adgrd1 were decreased (**Fig. S3B**) in whole-brain lysates.

PrP^C is physiologically cleaved by proteases and its soluble N-terminus is involved in Adgrg6 activation (Altmeppen *et al*, 2015; Altmeppen *et al*, 2013; Oliveira-Martins *et al*, 2010). In prion infections, soluble PrP^C may be converted into PrP^{Sc} and be unavailable for other functions. Hence, Adgrd1 signaling may be aberrant in prion infections. We tested this hypothesis by culturing HEK^{Adgrd1} cells in medium obtained conditioned by cerebellar organotypic cultured slices (COCS) of wild-type mice (C57BL6/J) treated with non-infectious brain homogenate (NBH) or infected with scrapie prions (Rocky Mountain Laboratory strain, passage 6; RML6) for 56 days. Conditioned medium from NBH-treated COCS may undergo physiological shedding and interact with Adgrd1. Indeed, HEK^{Adgrd1} cells incubated with conditioned medium from NBH treated COCS showed a decreased cAMP signal. However, conditioned medium from prion-infected COCS enhanced the cAMP signal (**Fig. 6A**). This suggests that shed PrP^C is sequestered in prion-infected COCS, thereby preventing its physiological actions. No increase in cAMP was observed in HEK293T cells treated with conditioned medium from prion-infected COCS, suggesting that the cAMP increase requires the presence of Adgrd1.

Ablation of Adgrd1 prevents neurodegeneration in ex-vivo slice cultures

We generated Adgrd1-deficient mice by injecting short-guide RNAs (sgRNA) targeting exon 4 of the Adgrd1 gene, along with mRNA encoding Cas9, into single-cell embryos. Genomic DNA was extracted from ear biopsies of F_0 offspring mice, and DNA sequencing of the Adgrd1 (**Fig. 6B**). The chosen line carries a deletion of 82 bp in exon 4 (composed of 96 bp) on both alleles, resulting in a frameshift mutation at residue 63 of Adgrd1 gene and in a premature termination codon after residue 74 (**Fig. S3C**). The ablation of Adgrd1 was confirmed by western blotting using anti-Adgrd1 antibodies (**Fig. S3D**). The founder mouse was bred to wild-type mice, and heterozygous mice were interbred to generate homozygous Adgrd1$^{-/-}$ mice.

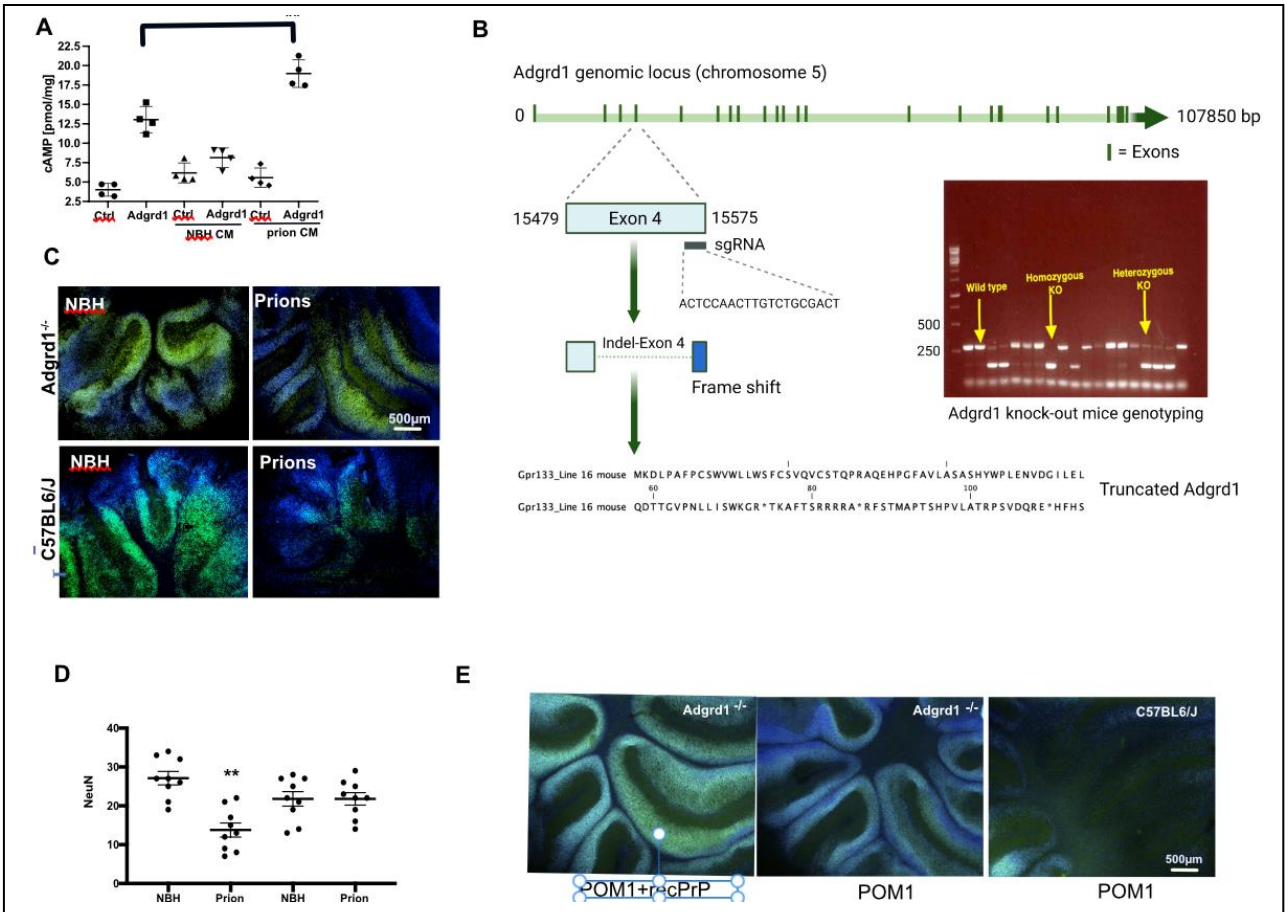

Figure 6: Adgrd1 ablation prevents prion-induced neurodegeneration. A: HEK293T cells were transiently transfected with control plasmid (pCDNA3) or with plasmid encoding Adgrd1 cDNA. 24 hours post transfection, cells were treated with conditioned medium from naïve or prion-infected COCS (56 dpi) for 24 hours. Conditioned medium from prion-infected COCS increased cAMP in Adgrd1-expressing cells but not in control cells. NBH CM: conditioned medium from NBH treated COCS. Prion CM: conditioned medium from prion-infected COCS. Unpaired-t test. **B:** Adgrd1$^{-/-}$ mice generation. Short-guide RNA (sgRNA) targeting exon 4 of Adgrd1 and mRNA encoding Cas9 were injected into single-cell embryos. Offspring were subjected to ear biopsies, and genomic DNA was sequenced to identify lines with ablated Adgrd1. For further studies, we chose a founder with a homozygous 77bp deletion in exon 4 causing frameshifting and premature termination of Adgrd1. Genotyping of heterozygous crossings using primers in the intronic regions flanking exon 4 revealed a 295-bp band in wild-type mice and a 170-bp band in ablated mice. **C:** Wild-type and Adgrd1$^{-/-}$ COCS were infected with prions (56 dpi) or exposed to NBH. Immunostaining was performed with anti-NeuN antibody (green) detecting neurons. After prion infection, morphometry revealed cerebellar granule cell loss in wild-type COCS but absence of neurodegeneration in Adgrd1$^{-/-}$ COCS. Each dot represents an individual slice. Nuclei were stained with DAPI. One-way Anova. **D:** Quantification of NeuN pixels (from C) was performed to assess neurodegeneration. Each dot represents a cerebellar slice. One-way Anova. **E:** COCS from 9-day-old mice pups were generated from the brains of C57BL6/J mice or Adgrd1 ablated mice. COCS were exposed to neurotoxic anti-PrP antibody POM1 or, for control, with recPrP-saturated POM1, cultured for 10 days, and stained with NeuN (green). POM1 triggered extensive neurodegeneration in Adgrd1^{h} but not in Adgrd1$^{-/-}$ COCS.

We generated cerebellar organotypic cultured slices (COCS) from 9-day old wild-type (C57BL6/J) and Adgrd1$^{-/-}$ mice. COCS were exposed to brain lysate (100 µg / insert) obtained from NBH or RML6 infected mice. At 56 dpi, COCS were immunostained with antibodies to NeuN, which identifies cerebellar granule cells, and assessed morphometrically to measure the neuronal loss. Wild-type COCS show decreased neuronal counts after prion infection, whereas Adgrd1$^{-/-}$ COCS did not show any signs of neurodegeneration (**Fig. 6C-D**). We next challenged Adgrd1$^{-/-}$ COCS with an anti-PrP antibody targeting globular domain (POM1) of prion protein and known to act as prion mimetic. Treatment with POM1 revealed neurodegeneration in wild-type COCS, but not in Adgrd1$^{-/-}$ COCS at 2 weeks post treatment (**Fig. 6E**).

Ablation of Adgrd1 delays onset of clinical symptoms observed in prion disease

We next investigated if Adgrd1 ablation prolongs the life span of prion-infected mice. Five wild-type (C57BL6/J) and six Adgrd1$^{-/-}$ mice were intracerebrally injected with prions, and progression of the disease was monitored. Wild-type mice infected with prions show motor coordination defects beginning at approx. week 19, as measured by rotarod performance tests (Sorce *et al*, 2020). We therefore tested prion-infected,

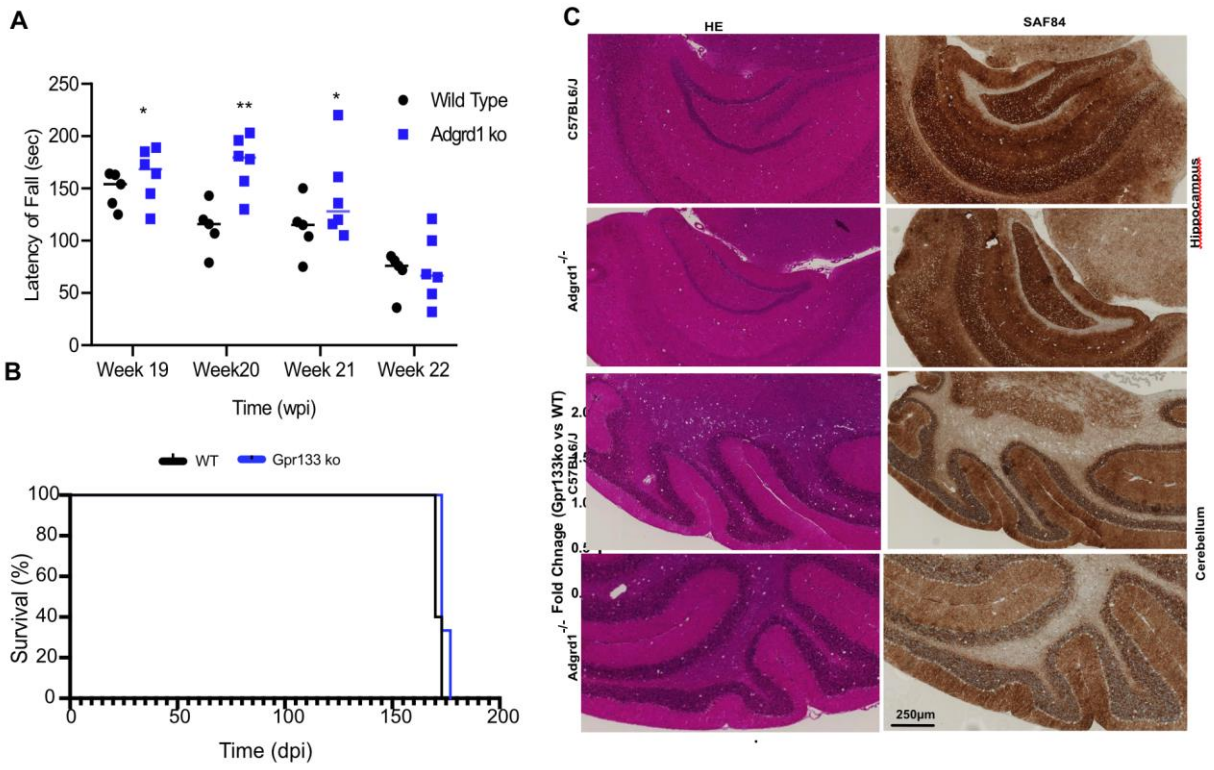

Figure 7: Ablation of Adgrd1 fails to prevent prion disease in mice. A: Motor coordination of prion-inoculated Adgrd1$^{+/+}$ and Adgrd1$^{-/-}$ mice was measured by rotarod. Adgrd1$^{-/-}$ mice showed better motor skills than Adgrd1$^{+/+}$ mice at weeks 19-21 post inoculation. After week 22, all mice performed poorly in the rotarod test. Dots: Latency to fall. Each dot represents an individual mouse. One-way Anova followed by Tukey's multiple comparison test. **B:** Survival curves of Adgrd1$^{+/+}$ (n=5) and Adgrd1$^{-/-}$ mice ablated mice (n=6) inoculated with RML6 prions intracerebrally. All mice developed clinical signs of prion disease. C57Bl6/J mice showed a median survival time of 170 days while Adgrd1 ablated mice showed a median survival time of 173 days. **C:** Whole brain sections from prion infected C57BL6/J and Adgrd1 ablated mice were immunostained with anti-PrP antibody SAF84. PrP^{Sc} deposits were seen in all mice. **D:** Hippocampal and cerebellar histology of prion-infected Adgrd1$^{+/+}$ and Adgrd1$^{-/-}$ mice. Sections were stained with hematoxylin and eosin (H&E) and SAF84 (anti-PrP) antibody. Both mouse strains showed conspicuous PrP^{Sc} deposition.

wild-type mice, and Adgrd1$^{-/-}$ mice for their motor coordination skills from week 19-22. Adgrd1$^{-/-}$ mice performed significantly better in motor coordination compared to wild-type mice during weeks 19-20, but at week 21 and thereafter all mice performed similarly poorly (**Fig. 7A**). These results suggest a delay in the onset of the symptoms in Adgrd1$^{-/-}$ mice. All mice eventually developed clinical signs of scrapie; wild-type mice had a median survival of 170 days compared to 173 days (p=0.0222) for Adgrd1$^{-/-}$ mice (**Fig. 7B**). Histological analysis revealed spongiform encephalopathy with PrP^{Sc} deposits in brains of both wild-type and Adgrd1$^{-/-}$ mice (**Fig. 7C**, **S4A**). Astrogliosis and microglial proliferation were prominent and did not vary between the two lines, suggesting that ablation of Adgrd1 does not affect the neuroinflammatory reactions to prion infection (**Fig. S4A**).

Discussion

These investigations were triggered by our previous finding that the N-terminal flexible tail of PrP^C (FT) transduces the toxicity caused by certain anti-PrP^C antibodies. The FT participates in several biological functions attributed to PrP^C, including the maintenance of peripheral nerve myelin (Bremer *et al*, 2010). The action of PrP^C in this context is non-cell-autonomous: the "flexible tail" (FT) of neuronal PrP^C is cleaved by regulated proteolysis, and the FT then activates Adgrg6 (Gpr126) on Schwann cells (Kuffer *et al.*, 2016). Conversely, the cell-autonomous activation of the FT in neurons is toxic (Wu *et al*, 2017). Because prion proteins can interact with several other receptors including the metabotropic glutamate receptors, we tested the ability of FT to bind to several other adhesion GPCRs that bear domain resemblance to Adgrg6. We discovered that the FT of the cellular prion protein regulates the activity of Adgrd1 (Gpr133), but not of any of the remaining adhesion GPCR tested. Since single-cell RNA sequencing databases indicate that Adgrd1 is exclusively expressed by a subset of neurons in the adult mouse brain, this finding raised the question whether its interaction with PrP^C might bear relevance to the pathogenesis of prion diseases.

Adgrd1 structurally resembles Adgrg6, having an extended extracellular domain containing the PTX and GAIN domains. Both receptors can be activated by a similar mechanism involving the displacement of an N-terminal fragment, which in turn unmasks a tethered agonist called the “Stachel” peptide (Liebscher *et al.*, 2015). The Stachel can fold back onto the receptor and activate it (Qu *et al*, 2022). Although the FT of PrP^C acts as an agonist of Adgrg6, our investigations revealed that FT suppresses the activity of Adgrd1.

Two scenarios can explain this finding. In a first scenario, Adgrd1 is constitutively active and is rendered inactive by its interaction with FT. In this case, FT would act as an inverse agonist. Alternatively Adgrd1 is activated by a hitherto unidentified endogenous ligand, and the displacement of this hypothetical ligand by FT quenches its activity. In this scenario FT acts as a true antagonist devoid of intrinsic activity. We have attempted to discriminate between these two possibilities using chimeric receptors in which we mounted the N-terminal fragment of Adrgrd6 onto the 7-transmembrane domain of Adgrg1, and vice versa. We originally envisaged that these chimeras might deliver insights into the receptor domains specifying positive vs. negative modulation by FT. Indeed, the chimeric receptor 133C revealed that the 7-transmembrane domain of Adgrd1 is a direct modulator of downstream signaling. Binding of FT may prevent a conformational change within the receptor necessary for activation. Instead, the chimeric receptor 133N was found to be functionally dead, as it did not affect cAMP levels in the presence or absence of FT. However, when co-expressed with wild-type Adgrd1, 133N prevented dose-dependently the cAMP spike in the absence of FT. This surprising finding suggests that 133N competes with Adgrd1 for a hitherto uncharacterized endogenous ligand via its extracellular domain. If so, FT might act as a true antagonist rather than an inverse agonist, and reduce Adgrd1 activity by displacing its physiological agonist.

Coupling of Adgrd1 to the Gs heterotrimer was further confirmed by in vitro experiments with purified components. Formation of the complex was only detected when Stachel was added. This suggests that Adgrd1

without additional Stachel peptide is activated, as confirmed by the cellular signaling data, but this Adgrd1 might only form the complex transiently. By adding Stachel, Adgrd1 may not only enhance its signaling activity but may also form a more stable complex amenable to purification. Our cryo-EM analysis shows that Adgrd1 with the additional Stachel peptide binds the mini-Gs protein heterotrimer to form an active signaling complex. Activation of the Gs pathway subsequently leads to a cAMP increase in cells as shown in our overexpression experiments. Constitutively high cAMP in the cells can induce cytotoxicity (Walia *et al*, 2018). Our data here suggests that FT regulates Adgrd1 cAMP-mediated signaling by functioning as an antagonist.

At the molecular level, FT binds to Adgrd1 via its charged cationic domain presumably to both the GAIN and PTX domains, resulting in suppression of receptor activity and thereby of cAMP induction. Interestingly, it is the positive charge imparted by the cationic domain of FT rather than its sequence that is required for the modulation of receptor activity. Such electrostatic mode of interactions between the ligands and receptors has also previously been observed in the case of other GPCRs such as the relaxin family receptors and C-C chemokine receptor type 5 (CCR5) (Wang *et al*, 2019; Zhang *et al*, 2021).

The KKRPKPG polycationic cluster within the N-proximal region of FT is highly conserved across species, suggesting that it has an important function. Moreover, mice lacking the polycationic cluster showed a delayed onset of prion disease (Turnbaugh *et al*, 2012), suggesting that it plays a role in prion pathogenesis. The absence of serious central nervous system disease in mice devoid of PrP does not exclude the possibility that loss of PrP^{C} function contributes to prion pathogenesis. The results presented above indicate that one such function may be the suppression of excessive Adgrd1 signaling ultimately resulting in cytotoxicity.

We investigated the latter question by infecting Adgrd1-deficient COCS with prions. These slices were resistant to neuronal loss induced by prions, indicating that Adgrd1 does indeed contribute to neurotoxicity. Adgrd1 ablation significantly improved the locomotory functions of prion-infected mice until the late stage of the disease, even if it only marginally extended their survival. These findings indicate that removal of Adgrd1 extends the healthspan but not the lifespan of mice, in accordance with the hypothesis that it acts downstream of prion replication as a mediator of prion toxicity. Consequently, prion replication proceeds unabated in Adgrd1-ablated mice, eventually leading to terminal disease and death similarly to what was observed in mice lacking the type-1 metabotropic glutamate receptors mGluR1 and mGluR5 (Goniotaki *et al.*, 2017). Indeed the deposition of PrP^{Sc} in brains of prion-infected mice was indistinguishable between wild-type and Adgrd1-deficient mice. Although combined healthspan and lifespan extension is the ultimate goal for humans suffering from prion disease, improvements in the quality of life during disease progression would also be highly desirable.

.

Acknowledgements

We thank Davide Caredio, Rita Moos, Mirzet Delic, Petra Schwarz, Emiliya Poghosyan, Elisabeth Agnes Müller Gubler, Jonas Mühle and Rajlakshmi Marpakwar for help, members of Aguzzi lab and Schertler lab for discussions, Giulia Miracca for help with illustrations, the Center for Microscopy and Image Analysis of the University of Zurich, the Scientific Center for Optical and Electron Microscopy at ETH Zurich, and Pavel Afanasyev for cryo-EM technical support. We are grateful to Kausthubh Ramachandran for performed the sequence alignment and analysis of the KKRPKPGG motif from various species.

Funding

AA is the recipient of an Advanced Grant of the European Research Council (ERC 670958) and of grants of the Swiss National Foundation (SNF 179040), the Nomis Foundation, the Human Frontiers Science Program and SwissUniversities. AKKL is the recipient of a grant from the Synapsis Foundation. GFXS is the recipient of a grant from the Synapsis Foundation (2018-PI04). AA and GFXS are co-recipients of a Swiss National Foundation Sinergia grant (CRSII5_183563). XD is the recipient of a Swiss National Foundation grant (SNF 192780).

Author contributions

AKKL, OT, CJT and AA designed the experiments and wrote the manuscript. AA and GFXS initiated and supervised the project. AKKL performed, or contributed to, all experiments including western blots, cAMP ELISA experiments on cerebellar organotypic cultured slices (COCS), immunofluorescence, imaging, Rotarod Assays. OT and CJT performed construct design and biochemical experiments of the Adgrd1-mini Gs complex. OT and JM performed the cryo-EM studies of the Adgrd1-mini Gs complex. OT, CJT, XD and GFXS analyzed the structure and proposed a molecular mechanism of signaling. RGG and XD built and analyzed the computational structural models. EDC contributed to cell viability assays. MJ contributed to the cAMP assays and generation of Adgrd1 mutants. RM contributed to Cell viability assays using Incucyte. SH contributed to generating recombinant PrP, FT and GD proteins.

Conflict of Interest: GFXS is a co-founder and scientific advisor of the companies leadXpro AG and InterAx Biotech AG.

References

Altmeppen HC, Prox J, Krasemann S, Puig B, Kruszewski K, Dohler F, Bernreuther C, Hoxha A, Linsenmeier L, Sikorska B *et al* (2015) The sheddase ADAM10 is a potent modulator of prion disease. *Elife* 4

Altmeppen HC, Prox J, Puig B, Dohler F, Falker C, Krasemann S, Glatzel M (2013) Roles of endoproteolytic alpha-cleavage and shedding of the prion protein in neurodegeneration. *FEBS J* 280: 4338-4347

Baron U, Bujard H (2000) Tet repressor-based system for regulated gene expression in eukaryotic cells: principles and advances. *Methods Enzymol* 327: 401-421

Bayin NS, Frenster JD, Kane JR, Rubenstein J, Modrek AS, Baitalmal R, Dolgalev I, Rudzenski K, Scarabottolo L, Crespi D *et al* (2016) GPR133 (ADGRD1), an adhesion G-protein-coupled receptor, is necessary for glioblastoma growth. *Oncogenesis* 5: e263

Brandner S, Raeber A, Sailer A, Blattler T, Fischer M, Weissmann C, Aguzzi A (1996) Normal host prion protein (PrPC) is required for scrapie spread within the central nervous system. *Proc Natl Acad Sci U S A* 93: 13148-13151

Bremer J, Baumann F, Tiberi C, Wessig C, Fischer H, Schwarz P, Steele AD, Toyka KV, Nave KA, Weis J *et al* (2010) Axonal prion protein is required for peripheral myelin maintenance. *Nat Neurosci* 13: 310-318

Bueler H, Aguzzi A, Sailer A, Greiner RA, Autenried P, Aguet M, Weissmann C (1993) Mice devoid of PrP are resistant to scrapie. *Cell* 73: 1339-1347

Carpenter B, Tate CG (2016) Engineering a minimal G protein to facilitate crystallisation of G protein-coupled receptors in their active conformation. *Protein Eng Des Sel* 29: 583-594

Fischer L, Wilde C, Schoneberg T, Liebscher I (2016) Functional relevance of naturally occurring mutations in adhesion G protein-coupled receptor ADGRD1 (GPR133). *BMC Genomics* 17: 609

Fischer M, Rulicke T, Raeber A, Sailer A, Moser M, Oesch B, Brandner S, Aguzzi A, Weissmann C (1996) Prion protein (PrP) with amino-proximal deletions restoring susceptibility of PrP knockout mice to scrapie. *EMBO J* 15: 1255-1264

Frenster JD, Kader M, Kamen S, Sun J, Chiriboga L, Serrano J, Bready D, Golub D, Ravn-Boess N, Stephan G *et al* (2020) Expression profiling of the adhesion G protein-coupled receptor GPR133 (ADGRD1) in glioma subtypes. *Neurooncol Adv* 2: vdaa053

Goniotaki D, Lakkaraju AKK, Shrivastava AN, Bakirci P, Sorce S, Senatore A, Marpakwar R, Hornemann S, Gasparini F, Triller A *et al* (2017) Inhibition of group-I metabotropic glutamate receptors protects against prion toxicity. *PLoS Pathog* 13: e1006733

Khosravani H, Zhang Y, Tsutsui S, Hameed S, Altier C, Hamid J, Chen L, Villemaire M, Ali Z, Jirik FR *et al* (2008) Prion protein attenuates excitotoxicity by inhibiting NMDA receptors. *J Cell Biol* 181: 551-565

Kroeze WK, Sassano MF, Huang XP, Lansu K, McCorvy JD, Giguere PM, Sciaky N, Roth BL (2015) PRESTO-Tango as an open-source resource for interrogation of the druggable human GPCRome. *Nat Struct Mol Biol* 22: 362-369

Kuffer A, Lakkaraju AK, Mogha A, Petersen SC, Airich K, Doucerain C, Marpakwar R, Bakirci P, Senatore A, Monnard A *et al* (2016) The prion protein is an agonistic ligand of the G protein-coupled receptor Adgrg6. *Nature* 536: 464-468

Liebscher I, Schon J, Petersen SC, Fischer L, Auerbach N, Demberg LM, Mogha A, Coster M, Simon KU, Rothemund S *et al* (2015) A Tethered Agonist within the Ectodomain Activates the Adhesion G Protein-Coupled Receptors GPR126 and GPR133. *Cell Rep* 10: 1021

Oliveira-Martins JB, Yusa S, Calella AM, Bridel C, Baumann F, Dametto P, Aguzzi A (2010) Unexpected tolerance of alpha-cleavage of the prion protein to sequence variations. *PLoS One* 5: e9107

Peggion C, Bertoli A, Sorgato MC (2011) Possible role for Ca2+ in the pathophysiology of the prion protein? *Biofactors* 37: 241-249

Ping YQ, Xiao P, Yang F, Zhao RJ, Guo SC, Yan X, Wu X, Zhang C, Lu Y, Zhao F *et al* (2022) Structural basis for the tethered peptide activation of adhesion GPCRs. *Nature* 604: 763-770

Prusiner SB (1982) Novel proteinaceous infectious particles cause scrapie. *Science* 216: 136-144

Qu X, Qiu N, Wang M, Zhang B, Du J, Zhong Z, Xu W, Chu X, Ma L, Yi C *et al* (2022) Structural basis of tethered agonism of the adhesion GPCRs ADGRD1 and ADGRF1. *Nature* 604: 779-785

Richard E, Michael ON, Alexander P, Natasha A, Andrew S, Tim G, Augustin Ž, Russ B, Sam B, Jason Y *et al* (2022) Protein complex prediction with AlphaFold-Multimer. *bioRxiv*: 2021.2010.2004.463034

Senatore A, Colleoni S, Verderio C, Restelli E, Morini R, Condliffe SB, Bertani I, Mantovani S, Canovi M, Micotti E *et al* (2012) Mutant PrP suppresses glutamatergic neurotransmission in cerebellar granule neurons by impairing membrane delivery of VGCC alpha(2)delta-1 Subunit. *Neuron* 74: 300-313

Sorce S, Nuvolone M, Russo G, Chincisan A, Heinzer D, Avar M, Pfammatter M, Schwarz P, Delic M, Muller M *et al* (2020) Genome-wide transcriptomics identifies an early preclinical signature of prion infection. *PLoS Pathog* 16: e1008653

Turnbaugh JA, Unterberger U, Saa P, Massignan T, Fluharty BR, Bowman FP, Miller MB, Supattapone S, Biasini E, Harris DA (2012) The N-terminal, polybasic region of PrP(C) dictates the efficiency of prion propagation by binding to PrP(Sc). *J Neurosci* 32: 8817-8830

Um JW, Kaufman AC, Kostylev M, Heiss JK, Stagi M, Takahashi H, Kerrisk ME, Vortmeyer A, Wisniewski T, Koleske AJ *et al* (2013) Metabotropic glutamate receptor 5 is a coreceptor for Alzheimer abeta oligomer bound to cellular prion protein. *Neuron* 79: 887-902

Walia MK, Taylor S, Ho PWM, Martin TJ, Walkley CR (2018) Tolerance to sustained activation of the cAMP/Creb pathway activity in osteoblastic cells is enabled by loss of p53. *Cell Death Dis* 9: 844

Wang JH, Nie WH, Shao XX, Li HZ, Hu MJ, Liu YL, Xu ZG, Guo ZY (2019) Exploring electrostatic interactions of relaxin family peptide receptor 3 and 4 with ligands using a NanoBiT-based binding assay. *Biochim Biophys Acta Biomembr* 1861: 776-786

Wu B, McDonald AJ, Markham K, Rich CB, McHugh KP, Tatzelt J, Colby DW, Millhauser GL, Harris DA (2017) The N-terminus of the prion protein is a toxic effector regulated by the C-terminus. *Elife* 6

Yao Z, van Velthoven CTJ, Nguyen TN, Goldy J, Sedeno-Cortes AE, Baftizadeh F, Bertagnolli D, Casper T, Chiang M, Crichton K *et al* (2021) A taxonomy of transcriptomic cell types across the isocortex and hippocampal formation. *Cell* 184: 3222-3241 e3226

Zhang H, Chen K, Tan Q, Shao Q, Han S, Zhang C, Yi C, Chu X, Zhu Y, Xu Y *et al* (2021) Structural basis for chemokine recognition and receptor activation of chemokine receptor CCR5. *Nat Commun* 12: 4151

Supplementary Figures

Figure S1

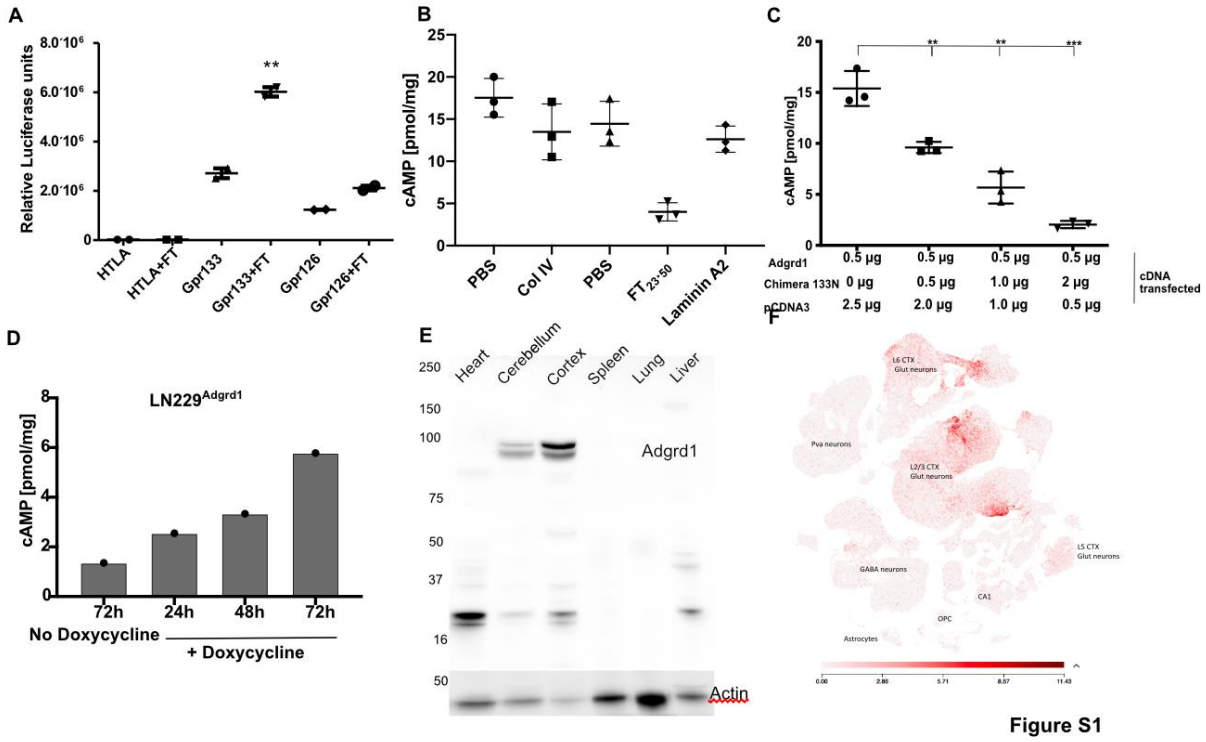

Figure S1

A: HTLA cells stably expressing the components of Presto-Tango Assay were transfected with Adgrd1 followed by treatment with FT (5uM; 6 hours). FT treated cells showed an increased luciferase accumulation suggesting the recruitment of arrestins upon FT treatment. As control Adgrd1 transfected cells were treated with PBS. To assess the background, luciferase accumulation in HEK cells was measured upon FT treatment.

B: HEK293T cells transiently transfected for 48h with Adgrd1 were exposed to either FT_{23-50}(2 µM; 30 min), Collagen IV (5g/ml; 20 min), or Laminin A2 (5µg/ml; 20 min). FT_{23-50} treated cells exhibited decreased cAMP levels. No change was observed in Collagen IV and Laminin A2 treated cells.

C: HEK293T cells were co-transfected with plasmids containing cDNA of either Adgrd1 and increasing concentrations of Chimera 133N. To equalize the total amount of transfected DNA to 3µg, pCDNA3 empty plasmid was also co-transfected in these cells. 48h post transfection cells were collected and intracellular cAMP levels were measured. Increasing concentrations of Chimera 133N, resulted in decreased cAMP accumulation and thereby acting as a dead receptor presumably by competing with Adgrd1 for endogenous ligand. Statistics: Unpaired t-test.

D: LN229 cells stably expressing Adgrd1 under doxycycline dependent (Tet-On) transcription control were either treated with doxycycline (2µg/ml) or not. Cells were collected at 24h, 48h and 72h post treatment and cAMP levels were measured using ELISA. As control, cAMP from cells plated for 72h but not exposed to doxycycline was used. Induction of Adgrd1 resulted in a progressive increase in cAMP levels.

E. Western blot analysis was performed on tissue lysates (50ug) using anti Adgrd1 antibody. Adgrd1 is expressed in cortex and cerebellum of the brain.

F: Heat map depicting the expression of Adgrd1 in different cell types of a mouse brain. Adgrd1 is expressed in subset of neuronal populations. Map was generated from single cell RNA sequencing data from the Allen brain atlas.

Figure S2

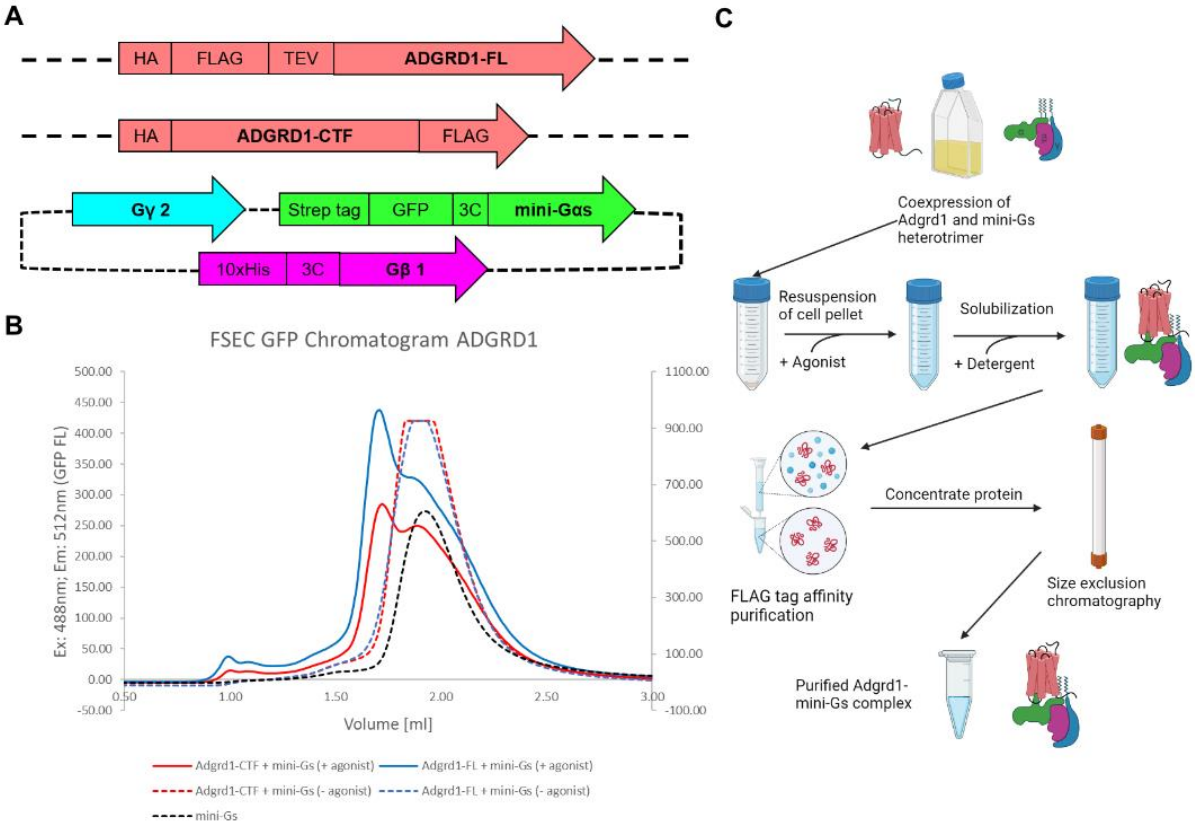

A. Design of the expression constructs used. Two constructs of Adgrd1 containing FL or CTF were designed (Top two panels). The expression vector for G protein heterotrimer contains mini-Gas, Gb and Gy (Bottom panel).

B. Analytical fluorescence size-exclusion chromatography was used to detect the GFP fluorescence from mini-Gas using excitation wavelength at 488 nm and emission wavelength at 512 nm. The following samples were measured: FL Adgrd1 mixed with mini-Gs with (red line) and without (red dash line) additional chemically synthesized stachel peptide. Adgrd1-CTF mixed with mini-Gs with (blue) and without (blue dash line) additional chemically synthesized stachel peptide. Black dash line represents the mini-Gs alone.

C. Workflow for preparing the complex of Adgrd1-CTF/mini-Gs heterotrimer. Figure made with Biorender.com

Figure S3

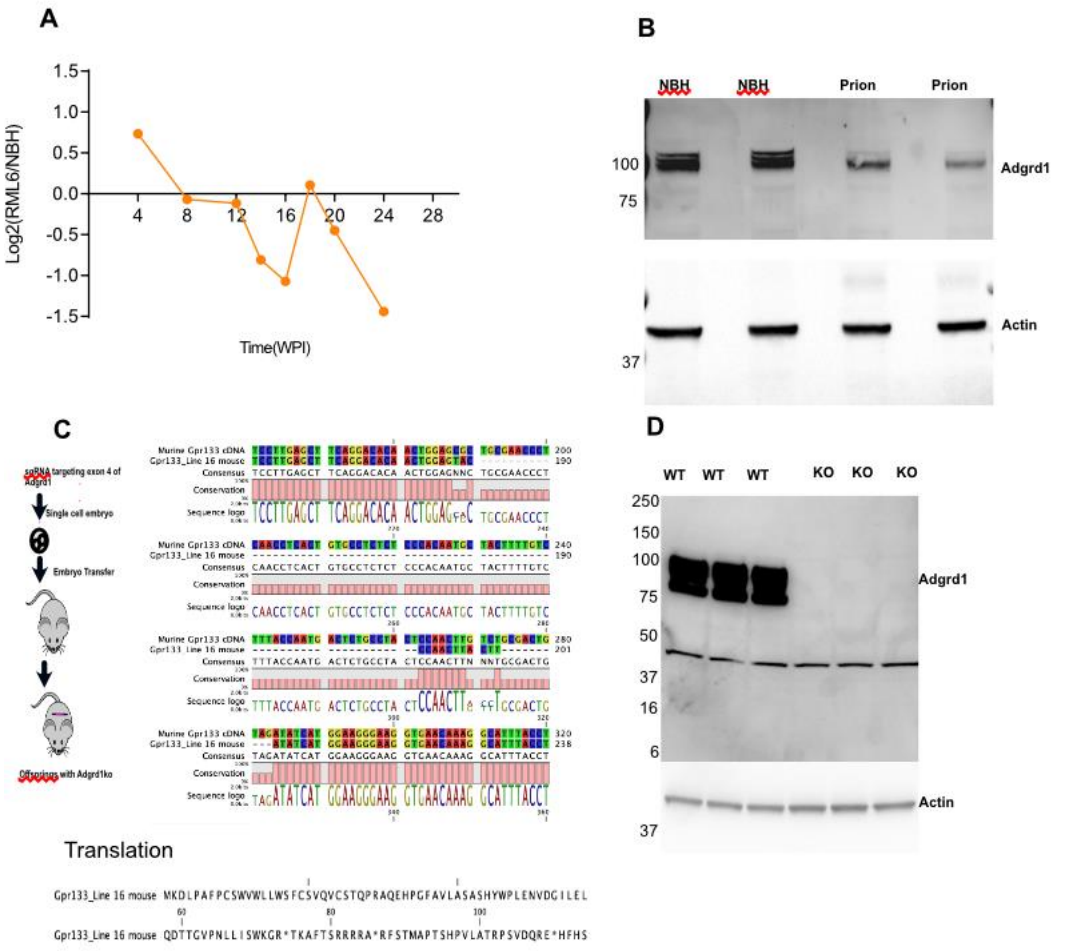

A : Expression levels of Adgrd1 mRNA during the course of prion disease. At terminal stage the expression level is decreased. Data was extracted from a longitudinal database of transcriptional changes during the course of prion disease in intracerebrally infected mice [1].

B: Western blot analysis on the total brain lysates (50µg) obtained from mice inoculated with prions or as controls with noninfectious brain homogenates, was performed using anti-Adgrd1 antibody. Actin was used as a loading control.

C: DNA sequence alignment between the wild type and Adgrd1 ablated mice reveals a 84bp deletion in Exon 4. The dotted line represents the deleted region and this resulted in a frame shift and premature stop codon. A short peptide of 73 amino acids is expected to be still generated.

D: Western blot analysis of the total brain lysates (50ug) from wild type and Adgrd1 ablated mice using anti Adgrd1 antibody. As expected mice ablated for Adgrd1 do not show expression of the protein as well as the presence of any shorter / truncated protein. Actin was used as a loading control.

Figure S4

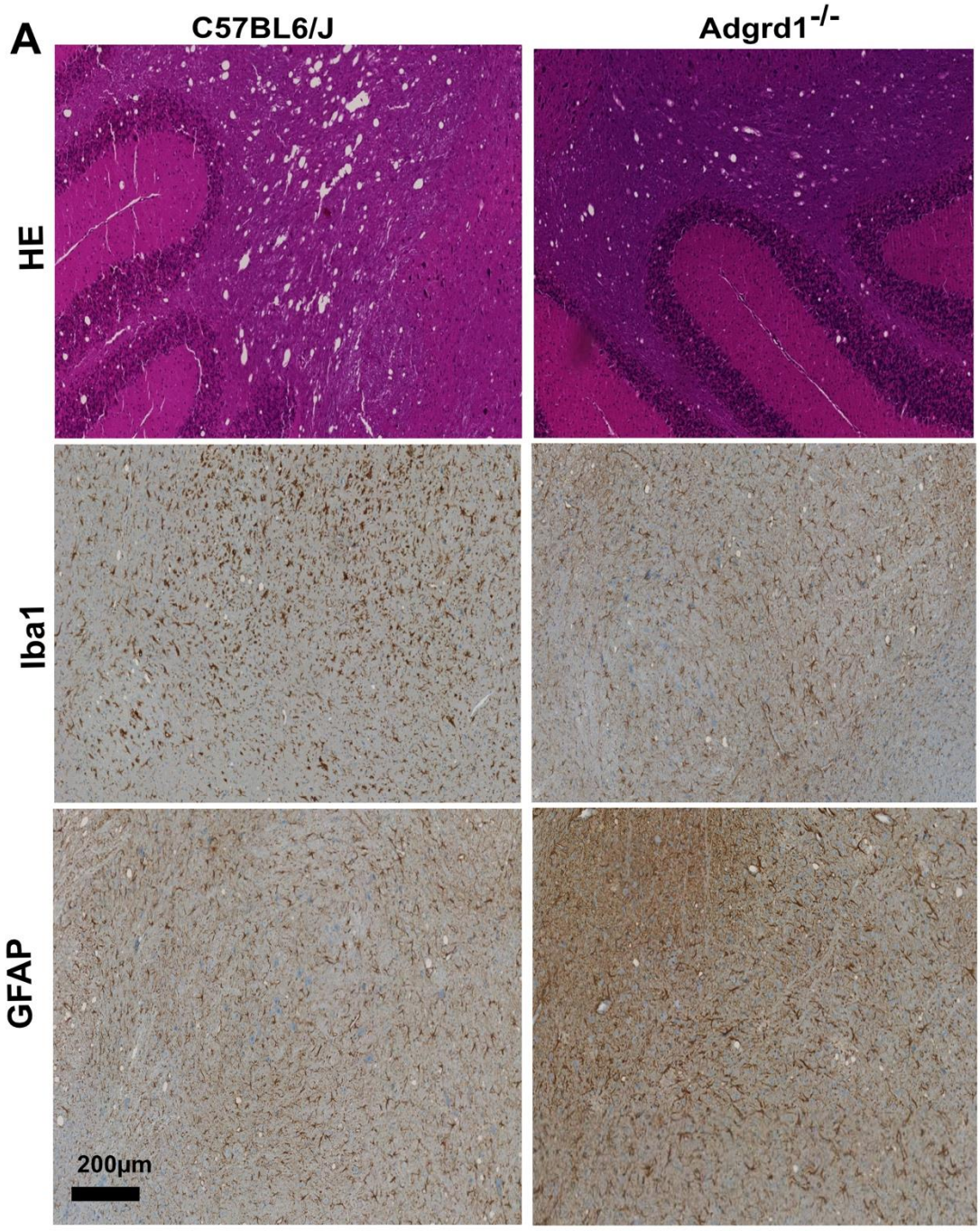

Histological analysis of prion-infected wild-type and Adgrd1 ablated mice. Both mice express classical signs of prion disease with extensive vacuolation, as observed with Haematoxylin and Eosin (H&E) staining. Both microglial proliferation (Iba1 staining) and Astrocytosis (GFAP staining) was also observed.

Figure S5

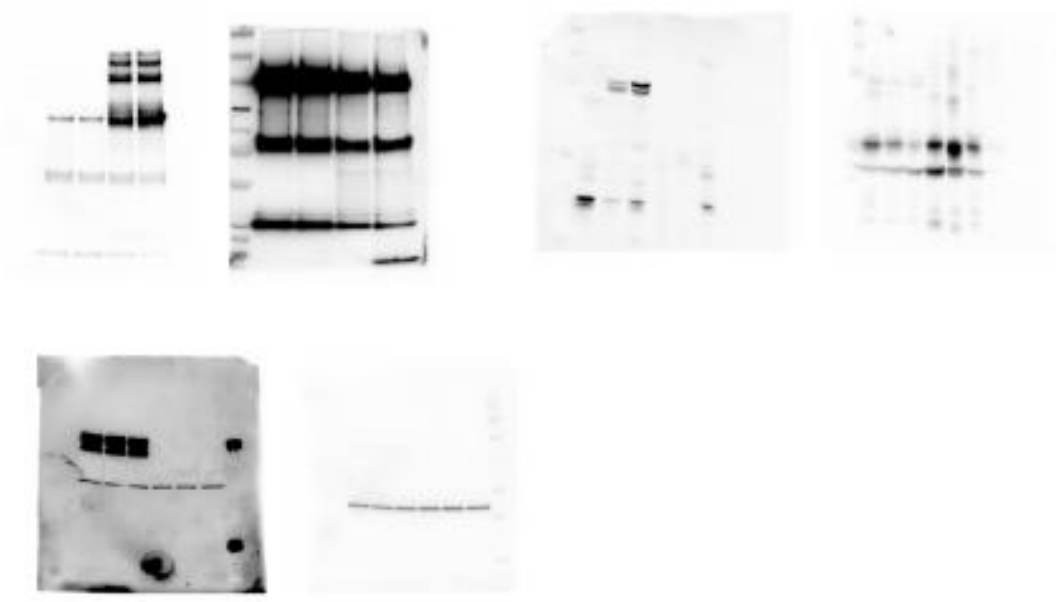

Figure S5

Raw, uncropped and unadjusted Western blots underlying the data shown in the manuscript.

Movies (GIF format)

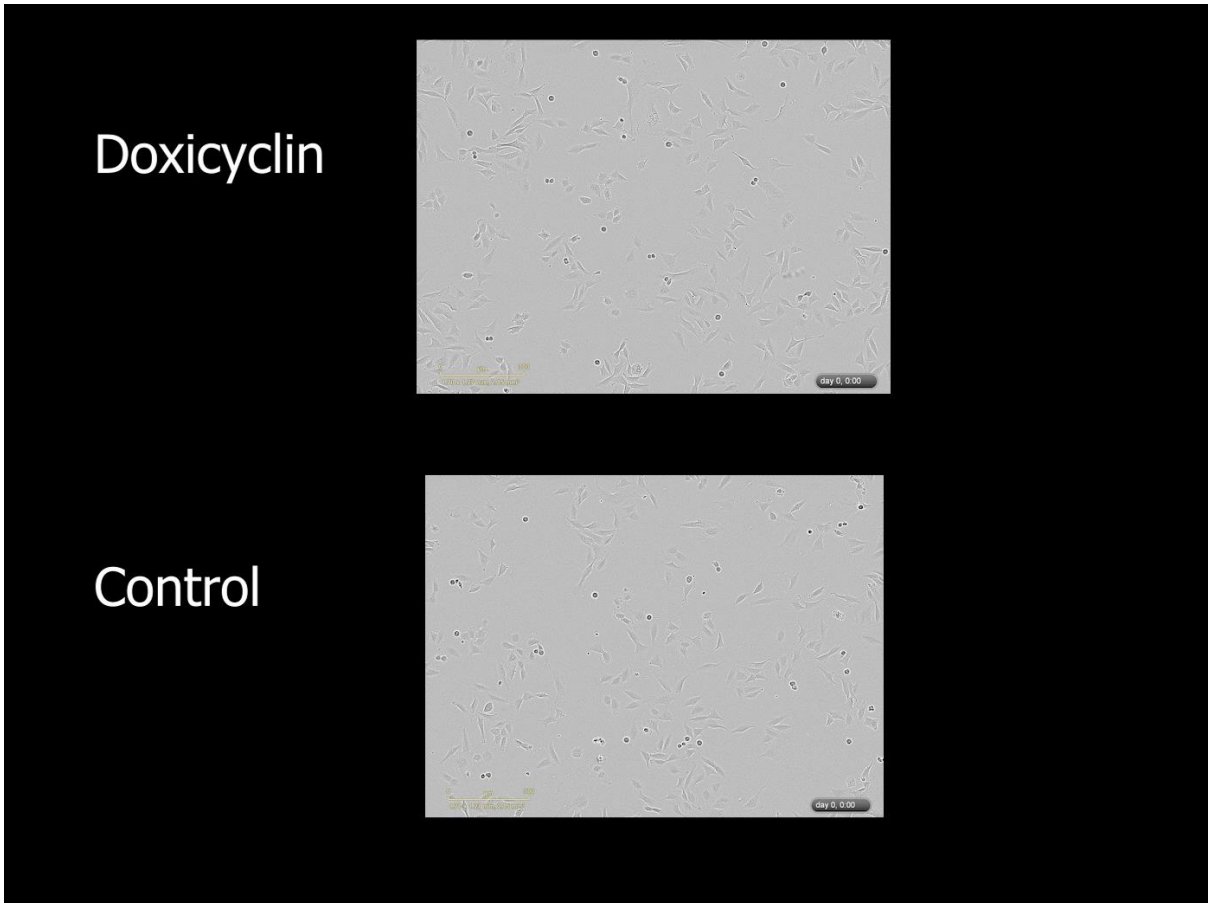

Movie S1: LN229 cells stably expressing Adgrd1 (LN229^{Adgrd1}) under the tetracycline responsive element were treated with doxycycline (2 µg/ml) to induce Adgrd1 expression. Cells were imaged every 4 hours for 9 days using Incucyte and a time course movie was generated using Image J. As control, LN229^{Adgrd1} cells, not treated with doxycycline were simultaneously imaged. Induction of Adgrd1 with doxycycline for 6 days results in extensive cell death suggesting that constitutive expression of Adgrd1 induced cellular toxicity.

Materials and Methods

Mice

Mice were bred in high hygienic grade facilities and housed in groups of 3-5, under a 12 h light/12 h dark cycle (from 7 am to 7 pm) at 21±1°C, with sterilized food (Kliba No. 3431, Provimi Kliba, Kaiseraugst, Switzerland) and water *ad libitum*. Animal care and experimental protocols were in accordance with the Swiss Animal Protection Law, and approved by the Veterinary office of the Canton of Zurich (permits ZH243/18 , ZH036/19). Mice of both genders were used in the current study.

The following mice were used in the current study: C57BL/6, *tga20* (B6;129-Tg(Prnp)a20Cwe Prnp<tm1Cwe>) and Adgrd1 knock out (C57BL/6J-Adgrd1<em1Aag>. Prions inoculations were performed by intracerebrally injecting RML6 prion strain described previously [2], with a dose corresponding to $3x10^5$ LD_{50} on 8 week old mice. Mice were sacrificed when full full blown clinical profile of scrapie was observed, As control non-infectious brain homogenate (NBH) was intracerebrally injected into the mice and they were sacrificed approximately at the same time as when the prion infected mice reach the terminal stage (at the latest time point compatible with humane euthanasia) of the disease.

Cell lines

Sf9 (*Spodoptera frugiperda*) and High Five (*Trichoplusia ni*) insect cells were obtained from Thermo Fisher Scientific. Both cell lines were cultured in Sf-900™ III serum-free medium (Thermo Fisher Scientific) at 27°C and 120 r.p.m. HEK293T, LN229 cells were cultured in DMEM supplemented with 10% fetal bovine serum (FBS), penicillin-streptomycin and Glutamax (all from Thermofisher). All cell lines were controlled for the presence of Mycoplasma contamination.

Peptide

The stachel-sequence derived peptide (TNFAILMQVVPLE) was synthesized at Peptide 2.0 (Chantilly, VA, USA).

Constructs

The cDNA encoding the human Adgrd1 (isoform 1, Uniprot ID: Q6QNK2-1) and the Adgrd1-CTF (residues T545-V874) were synthesized and cloned into pAC8REDNK vector (gift from Arnaud Poterszman [3]) at Genewiz (from Azenta Life Sciences). The Adgrd1-FL construct starts with an N-terminal haemagglutinin (HA) signal peptide (MKTIIALSYIFCLVFA) followed by a FLAG-tag (DYKDDDDA), a tobacco etch virus (TEV) protease cleavage site (ENLYFQG) and Adgrd1 (V26-V874). The Adgrd1-CTF contains residues T545-V874 with an N-terminal HA signal peptide and a C-terminal FLAG-tag (DYDKDDDDK). An engineered shortened human Gαs subunit (mini-Gαs 399)[4], which lacks the α-helical domain, was further modified with an N-terminal Strep-tag (WSHPQFEK) followed by a GFP and a HRV 3C cleavage sequence (LEVLFQG). The human $G\beta_1$ was modified with an N-terminal 10xHis tag followed by a HRV 3C cleavage sequence. The human $G\gamma_2$ was not further modified. All three G protein subunits were cloned into the pAC8REDNK vector for insect cell expression. Human Adgrd1 cDNA was obtained from Origene (Cat: PS100001). Generation of Adgrd1 N-terminal mutations was carried out using Q5 site directed mutagenesis kit (NE Biolabs) using manufacturers

protocol. Transfections were carried out in 6 well plates using Lipofectamine 3000 according to the manufacturer's instructions. 3ug of DNA was used for transfection per well.

Virus production and expression

High-titer recombinant baculovirus stocks were generated using the flashBAC™ expression system in Sf9 cells. 1.5 ug plasmid DNA was mixed with 500 ng linearized BAC10:KO1629 DNA (Oxford Expression Technologies Ltd.) and 8 ul Cellfectin™ II reagent (Thermo Fisher Scientific) in 200 ul Sf-900™ III serum-free medium with incubation for 20 min. The transfection mix was added to 1 x 10^6 Sf9 cells in an adherent culture plate and incubated for 120 h. The P_0-generation virus was harvested from the supernatant and used to infect a 10-ml suspension cell culture at 1 x 10^6 cells/ml density. Supernatant with P_1-generation virus was harvested by centrifugation after 72 h incubation while shaking at 27°C. The procedure was repeated with a 100-ml cell suspension volume to generate the final P_2-generation virus for protein expression. High Five cells were cultured to a density of 3 x 10^6 cells/ml and infected with viruses for Adgrd1 and mini-Gs heterotrimer at 1:1 (v/v) ratio. Cells were harvested after 48 h and cell pellets were stored at -80°C.

Complex purification

20 g of cell pellet was resuspended in 100 ml of 20 mM HEPES pH 7.5, 100 mM NaCl, 2 mM $MgCl_2$ and 1 mM DTT supplemented with DNase I (10 µg/ml) and complete protease inhibitor cocktail tablets (Roche). Complex formation was initiated by adding synthesized Stachel peptide (100 µM) and kept constant during the purification procedure. Incubation for 2 h at room temperature with the addition of apyrase (25 mU/ml) allowed complex formation on cell membrane. Solubilization was done by supplementing 1% (w/v) lauryl maltose neopentyl glycol (LMNG, Anatrace) and 0.1% (w/v) cholesteryl hemisuccinate (CHS, Anatrace) and incubation for 2 h at 4°C. Insoluble material was removed by centrifugation at 136'000xg for 45 min. The clarified supernatant was incubated overnight with 2 ml anti-DYKDDDDK G1 Affinity Resin (Genscript) at 4°C by batch binding. The resin was collected in a gravity flow column and washed with 30 column volumes of wash buffer (20 mM HEPES pH 7.5, 100 mM NaCl, 2 mM $MgCl_2$, 10% glycerol, 1mM DTT, 0.01% LMNG, 0.002% CHS and 0.002% glycol-diosgenin (GDN, Anatrace)). Complex was eluted using wash buffer supplemented with 0.2 mg/ml Flag peptide (Genscript). Eluent was concentrated and injected to a Superdex 200 increase 10/300 GL column (GE Healthcare) pre-equilibrated with 20 mM HEPES pH 7.5, 100 mM NaCl, 2mM $MgCl_2$, 0.001% LMNG, 0.0002% CHS and 0.0002% GDN. The fractions containing receptor-G protein complex were combined and used for cryo-EM grid preparation.

Cryo-EM grid preparation and data acquisition

A volume of 3 µl purified complex at a concentration of 1.5 mg/ml was applied to glow-discharged holey carbon grids (Quantifoil R1.2/1.3 Cu 200 mesh). The grids were blotted with a Vitrobot Mark IV (Thermo Fisher Scientific) and flash frozen in liquid ethane. The sample was blotted for 2s at 4°C and 100% humidity. Data was acquired on a 300kV Titan Krios (Thermo Fisher Scientific) at a magnification of 165'000x, corresponding to a pixel size of 0.51 Å. A GIF Quantum LS energy filter (Gatan) was operated with an energy slit width of 20 eV. Movies were recorded with a K3 direct electron detector (Gatan) with defocus values from -0.8 µm to -2 µm. A total number of 40 frames per movie were recorded with an accumulated dose of 55 $e^-/Å^2$. EPU (FEI, Thermo Fisher Scientific) was used for automated data acquisition.

Cryo-EM data processing

Cryo-EM data was processed using cryoSPARC v3.3.2 [5]. Raw movies were subjected to beam-induced motion correction using cryoSPARC's patch motion correction. For each micrograph, contrast transfer function (CTF) parameters were determined by patch CTF estimation. Initial particles were picked on a subset of all micrographs using Topaz particle picking software [6] with the general model ResNet8 and the particles were subjected to reference-free 2D classification with the default parameters. 2D class averages showing the Adgrd1-mini-Gs complex with the corresponding particles were selected and Topaz was used to train a model for automated particle picking. Automated picking on the full dataset yielded 915'922 particles. Particles were again subjected to reference-free 2D classification. A total of 95'413 particles grouped into 2D averages showing the Adgrd1-Gs heterotrimer complex.

Arrestin Signaling Assay

The generation of plasmids for this assay was previously described and obtained from Addgene [7]. HTLA cells (a HEK293 cell line stably expressing a tTA-dependent luciferase reporter and a β-arrestin2-TEV fusion gene) were provided by the laboratory of B. Roth (University of North Carolina, Chapel Hill). Cells were grown on 6 well plates (500,000 cells/well) and were transfected with Adgrd1-Tango plasmid. 24h post transfections, cells were washed with PBS and fresh medium containing recombinant FT (23-110 residues) was added to the cells at 10uM concentration. As control cells were treated with PBS: 6 hours post treatment, cells were processed with Bright-Glo luciferase system (Promega) according to the manufacturers protocol. 25ug of the cell lysate was in 200ul of assay mix. Luciferase was detected by chemiluminescence.

cAMP Assay

cAMP levels in cell and tissue lysates were measured using a direct cAMP ELISA Assay kit (Enzo Life Sciences). Sample preparation for ELISA and data analysis were performed as described previously [8].

Immunohistochemistry

Mice brains were fixed in formalin followed by treatment with concentrated formic acid to inactivate prions. Brain sections (app 2um) were generated and deparaffinized using graded alcohols followed by antigen retrieval using 10mM citrate buffer (pH 6). The presence of prion deposits was visualized using SAF84 antibody (1:200; SPI Bio). Microglia and Astrocyte proliferation was visualized by staining the brain sections using anti Iba1 (1:2500; WAKO) and anti GFAP antibody (1:1000 Agilent technologies). When appropriate the brain sections were counterstained with haematoxylin and eosin. The images were acquired using NanoZoomer scanner (Hamamatsu Photonics) and visualized using NanoZoomer digital pathology software.

Cerebellar organotypic cultured slices (COCS)

9-12 day old pups were used to generate COCS from both the wild type and Adgrd1 ablated mice [9]. Pups from Adgrd1 ablated mice were genotyped using the toe clips before generating slices to confirm the knockout on both alleles. Once generated, COCS were transferred onto inserted in 6 well plates

and COCS and maintained in a standard cell culture incubator (37°C, 5% CO2, 95% humidity) Fresh medium was replenished once every 3 days.

Prion inoculations and POM1 treatment of COCS

Freshly generated COCS were infected with Rocky Mountain laboratory strain 6 prions (RML6) or as a control with either non-infectious brain homogenate (NBH). COCS with prions were maintained for 56 days and fixed with 4% paraformaldehyde and staining with NeuN (to label cerebellar granule neurons) and DAPI (to label nuclei). For treatment of COCS with toxic anti-PrPC antibody (POM1), slices were treated with POM1 (67nM) or as a control with IgG for 10 days after a 2-week recovery period after generation of slices. Slices were fixed, imaged, and analyzed as described previously (Ref).

Western blotting

Homogenization of mouse brains was performed in a TissueLyserLT by using 10 volumes of lysis buffer (0.5% Nonidet P-40, 0.5% 3-[(3-cholamidopropyl)dimethylammonio]-1-propanesulfonate (CHAPS), protease inhibitors (complete Mini, Roche), phosphates inhibitors (PhosphoSTOP, Roche) in PBS). Lysates were transferred to microfuge tubes and centrifuged at 1000g for 5 min at 4°C to remove the cell debris. 40ug of protein was loaded on SDS PAGE (4-12% Novex NuPAGE) followed by transfer onto nitrocellulose membrane using iBlot (Invitrogen). For proteins < 100 kDa, the transfer was performed at 20 V for 7 min. For proteins larger than 100 kDa, the transfer was performed at 15 V for 15 min. Samples were blocked in SureBloc (Lubio biosciences) for 1 hour followed by incubation with primary antibodies (anti Gpr133 antibody -Aviva Biosystems; anti Flag antibody: Sigma). HRP tagged Secondary antibodies: Goat Anti-Mouse IgG (H + L; #62-6520) or Peroxidase-Goat Anti-Rabbit IgG (H + L; #111.035.045) were used at 1:4000 for 1 h at room temperature and membranes were developed using Luminata Crescendo (Millipore). Images were acquired using Fusion Solo 7S Edge (Vilber).

Immunoprecipitations

HEK293T cells growing in 6 well plated were transfected with plasmid expressing Adgrd1 or as a control with pCDNA3. 24 hours post transfections, cells were washed twice with PBS followed by treatment with recombinant FT (10uM, 20min) or as control with PBS. Cells were washed with PBS and lysed in IP buffer: 1% Triton X-100 in PBS, 1× protease inhibitors (Roche) and Phosphostop (Roche) for 20 min on ice followed by centrifugation at 5000rpm for 5 min at 4°C. BCA assay was performed to quantify the protein and 1mg of protein was used for immunoprecipitation. 2mg of anti- Flag antibody was added to the cell lysate and incubated on the rotating wheel (overnight at 4°C). Following day, Protein G Dynabeads (25ul) was added per tube and further incubated on the rotating wheel for3h at 4°C. IP buffer was used to wash the beads (3 times, 5 min each) and after the final wash, sample buffer (containing 1mM DTT) was directly added to the beads. Samples were heated to 65°C for 20 minutes followed by SDS PAGE and western blotting with anti-Flag and anti PrP antibody (POM2).

Phylogenetic analyses

The sequence used for the human *PRNP* protein has the UniProt ID P04156 (referred to as PrP henceforth). The sequence of the isoform annotated as canonical was selected for the analysis. Homologs for PrP were detected using PSI-BLAST which was run for 5 iterations on the online BLAST server with default parameters [10, 11]. The search was performed on the RefSeq Protein database and the results were restricted to the *Mammalia* taxonomy (tax ID 40674). Only the putative homologs with a query cover between 90-100% and query identity between 75-100% were included in the PSI-BLAST iterations. This resulted in 164 putative homologs at the end of 5 iterations.

The sequences of the 164 putative homologs were downloaded from BLAST and aligned using MAFFT v7.453 using the E-INS-I option [12, 13]. The command used was "mafft --maxiterate 1000 --genafpair --reorder <alignment_file>.fasta > <aligned_file>.phy". One sequence (XP_011796434.1 - *Colobus angolensis palliatus* major prion protein isoform X5) was noted to have misalign with the rest of the alignment in the region of the motif of interest (KKRPKPGG) and was removed and the entire set was realigned. The alignment was visualized in Jalview [14] and the consensus sequence and consensus conservation percentages were extracted. The consensus sequence logo for the sequence between positions 123 and 135 was set to the Clustal colouring scheme and generated using WebLogo [15]. The plots were generated using Microsoft Excel. The KKRPKPGG motif was found to be highly conserved within *Mammalia.* In 57.4% (93 out of 162) of the sequences, the motif was KKRPKPGGG.

Molecular modelling

The sequences of the N-terminal fragment (residues 1 to 560) of human Adgr1 (Uniprot ID: Q6QNK2) and of FT_{23-50} were used to perform the prediction of the three-dimensional structure of the Adgr1-FT_{23-50} complex using AlphaFold Multimer v2.2.0 using default parameters. The flexible protein-peptide docking computational experiments were performed using the three-dimensional structure of the human Adgr1 N-terminus, as predicted by AlphaFold [16]. This structure was obtained by downloading complete human Adgrd1 prediction from the AlphaFold database [17] and extracting the N-terminal fragment with the molecular graphics program VMD [18]. The sequence of FT_{23-50} was then docked to that structure using the CABS-dock web server [19] with default parameters. Images were rendered using VMD [18] and the PyMOL Molecular Graphics System, Version 2.5.2 Schrödinger, LLC.

References

1. Sorce, S., et al., *Genome-wide transcriptomics identifies an early preclinical signature of prion infection.* PLoS Pathog, 2020. **16**(6): p. e1008653.
2. Zhu, C., et al., *SARM1 deficiency up-regulates XAF1, promotes neuronal apoptosis, and accelerates prion disease.* J Exp Med, 2019. **216**(4): p. 743-756.
3. Abdulrahman, W., et al., *A set of baculovirus transfer vectors for screening of affinity tags and parallel expression strategies.* Anal Biochem, 2009. **385**(2): p. 383-5.
4. Tate, B.C.C.G., *Engineering a minimal G protein to facilitate crystallisation of G protein-coupled receptors in their active conformation.* Protein Engineering, Design and Selection, 2016. **29**(12): p. 583-594.
5. Punjani, A., et al., *cryoSPARC: algorithms for rapid unsupervised cryo-EM structure determination.* Nat Methods, 2017. **14**(3): p. 290-296.
6. Bepler, T., et al., *Positive-unlabeled convolutional neural networks for particle picking in cryo-electron micrographs.* Nat Methods, 2019. **16**(11): p. 1153-1160.
7. Kroeze, W.K., et al., *PRESTO-Tango as an open-source resource for interrogation of the druggable human GPCRome.* Nat Struct Mol Biol, 2015. **22**(5): p. 362-9.
8. Kuffer, A., et al., *The prion protein is an agonistic ligand of the G protein-coupled receptor Adgrg6.* Nature, 2016. **536**(7617): p. 464-8.
9. Falsig, J., et al., *Prion pathogenesis is faithfully reproduced in cerebellar organotypic slice cultures.* PLoS Pathog, 2012. **8**(11): p. e1002985.
10. Altschul, S.F., et al., *Gapped BLAST and PSI-BLAST: a new generation of protein database search programs.* Nucleic Acids Res, 1997. **25**(17): p. 3389-402.
11. Schaffer, A.A., et al., *Improving the accuracy of PSI-BLAST protein database searches with composition-based statistics and other refinements.* Nucleic Acids Res, 2001. **29**(14): p. 2994-3005.

12. Katoh, K., et al., *Improvement in the accuracy of multiple sequence alignment program MAFFT.* Genome Inform, 2005. **16**(1): p. 22-33.
13. Katoh, K. and D.M. Standley, *MAFFT multiple sequence alignment software version 7: improvements in performance and usability.* Mol Biol Evol, 2013. **30**(4): p. 772-80.
14. Waterhouse, A.M., et al., *Jalview Version 2--a multiple sequence alignment editor and analysis workbench.* Bioinformatics, 2009. **25**(9): p. 1189-91.
15. Crooks, G.E., et al., *WebLogo: a sequence logo generator.* Genome Res, 2004. **14**(6): p. 1188-90.
16. Jumper, J., et al., *Highly accurate protein structure prediction with AlphaFold.* Nature, 2021. **596**(7873): p. 583-589.
17. Varadi, M., et al., *AlphaFold Protein Structure Database: massively expanding the structural coverage of protein-sequence space with high-accuracy models.* Nucleic Acids Res, 2022. **50**(D1): p. D439-D444.
18. Humphrey, W., A. Dalke, and K. Schulten, *VMD: visual molecular dynamics.* J Mol Graph, 1996. **14**(1): p. 33-8, 27-8.
19. Edgar, R.C., *MUSCLE: multiple sequence alignment with high accuracy and high throughput.* Nucleic Acids Res, 2004. **32**(5): p. 1792-7.

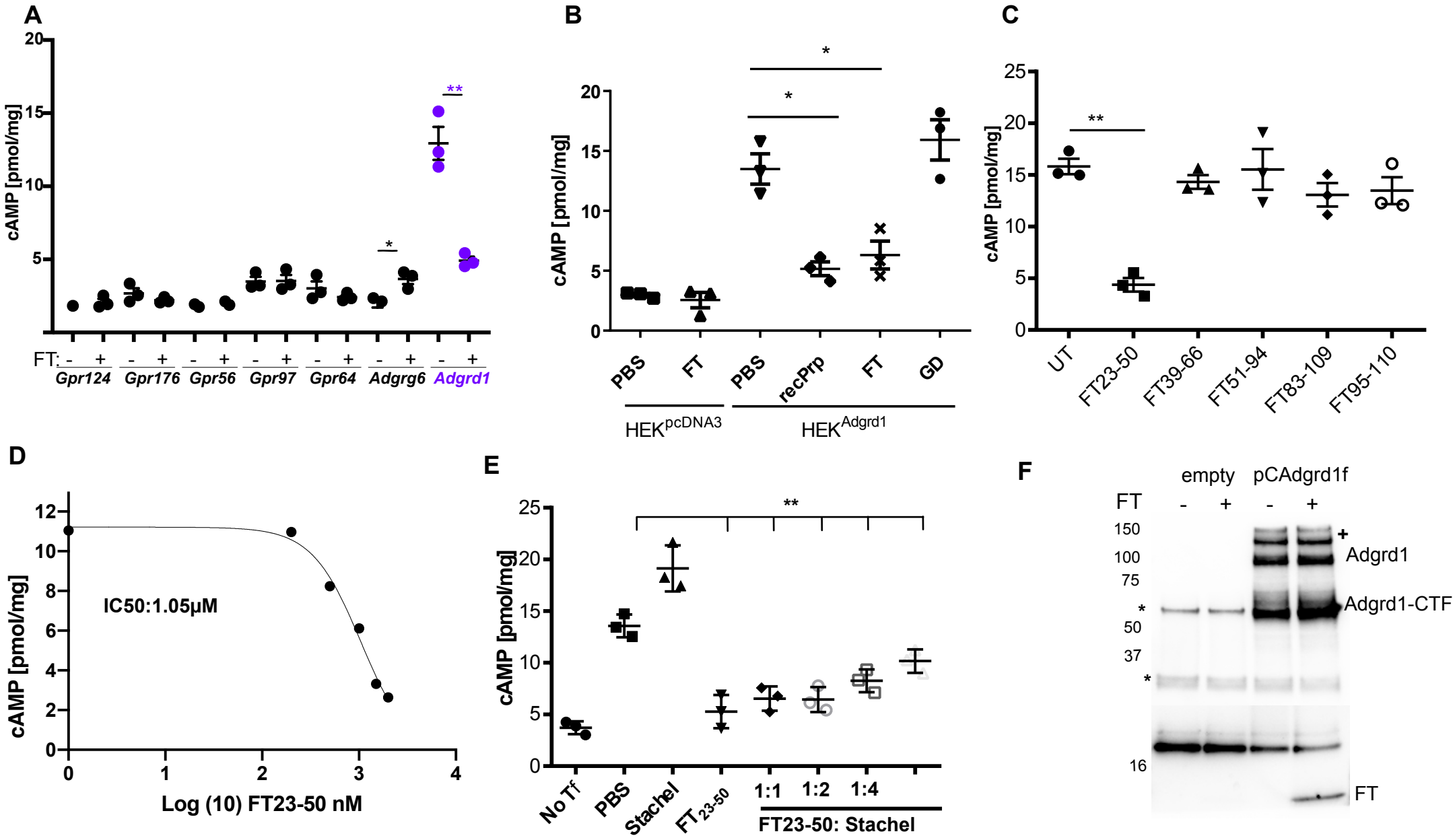
A
cAMP [pmol/mg]
FT: - + - + - + - + - + - + - +
Gpr124 Gpr176 Gpr56 Gpr97 Gpr64 Adgrg6 Adgrd1
B
cAMP [pmol/mg]
PBS FT PBS recPrp FT GD
HEKpcDNA3
HEKAdgrd1
C
cAMP [pmol/mg]
UT FT23-50 FT39-66 FT51-94 FT83-109 FT95-110
D
cAMP [pmol/mg]
IC50:1.05µM
Log (10) FT23-50 nM
E
cAMP [pmol/mg]
No Tf PBS Stachel FT23-50 1:1 1:2 1:4
FT23-50: Stachel
F
empty pCAdgrd1f
FT - + - +
150
100
75
50
37
16
Adgrd1
Adgrd1-CTF
FT

Figure 1

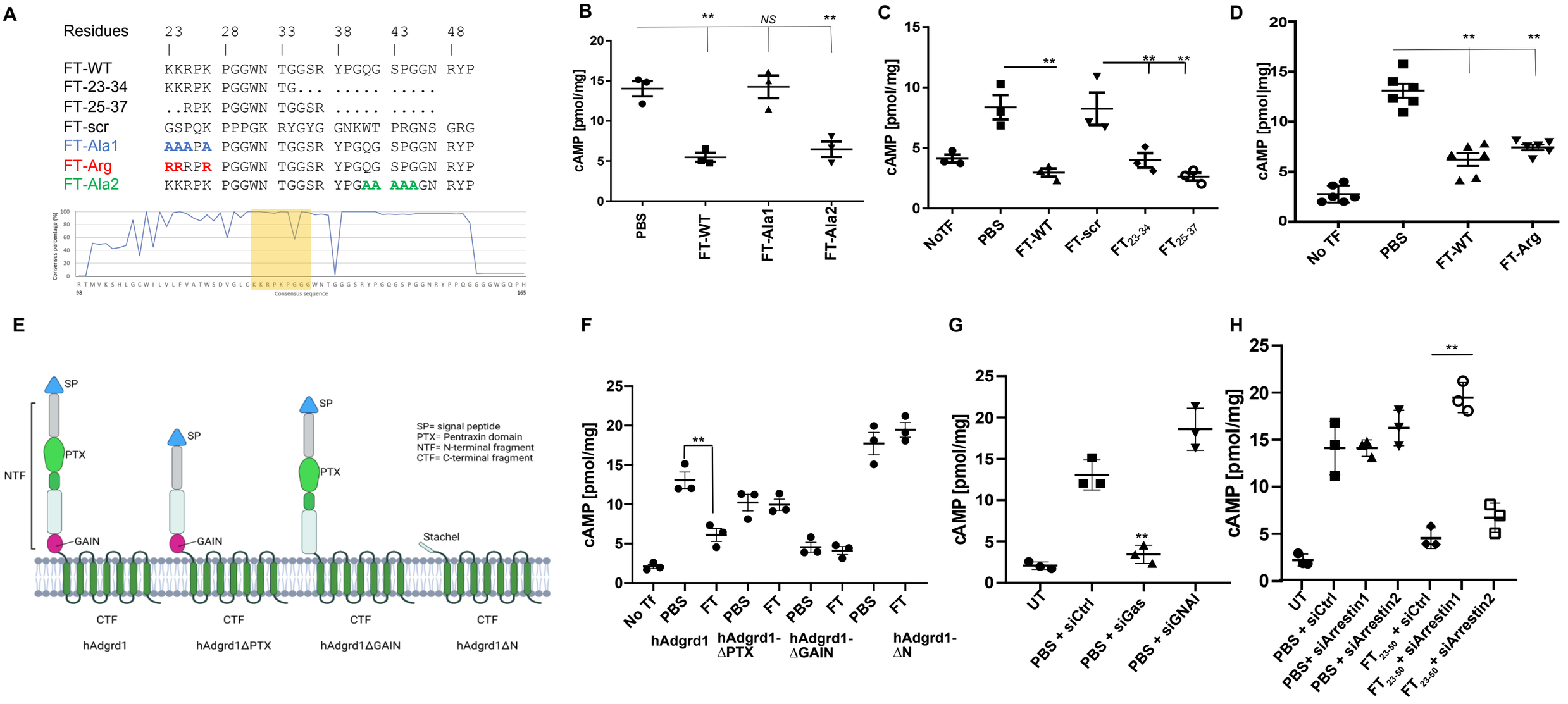
A
Residues 23 28 33 38 43 48
FT-WT KKRPK PGGWN TGGSR YPGQG SPGGN RYP
FT-23-34 KKRPK PGGWN TG... ....
FT-25-37 ..RPK PGGWN TGGSR ....
FT-scr GSPQK PPPGK RYGYG GNKWT PRGNS GRG
FT-Ala1 AAAPA PGGWN TGGSR YPGQG SPGGN RYP
FT-Arg RRRPR PGGWN TGGSR YPGQG SPGGN RYP
FT-Ala2 KKRPK PGGWN TGGSR YPGAA AAAGN RYP
Consensus percentage (%)
Consensus sequence
B
cAMP [pmol/mg]
PBS
FT-WT
FT-Ala1
FT-Ala2
NS
C
cAMP [pmol/mg]
NoTF
PBS
FT-WT
FT-scr
FT23-34
FT25-37
D
cAMP [pmol/mg]
No TF
PBS
FT-WT
FT-Arg
E
SP
PTX
NTF
GAIN
Stachel
CTF
SP= signal peptide
PTX= Pentraxin domain
NTF= N-terminal fragment
CTF= C-terminal fragment
hAdgrd1
hAdgrd1ΔPTX
hAdgrd1ΔGAIN
hAdgrd1ΔN
F
cAMP [pmol/mg]
No Tf
PBS
FT
hAdgrd1
hAdgrd1-ΔPTX
hAdgrd1-ΔGAIN
hAdgrd1-ΔN
G
cAMP [pmol/mg]
UT
PBS + siCtrl
PBS + siGas
PBS + siGNAI
H
cAMP [pmol/mg]
UT
PBS + siCtrl
PBS+ siArrestin1
PBS + siArrestin2
FT23-50 + siCtrl
FT23-50 + siArrestin1
FT23-50 + siArrestin2

Figure 2

A

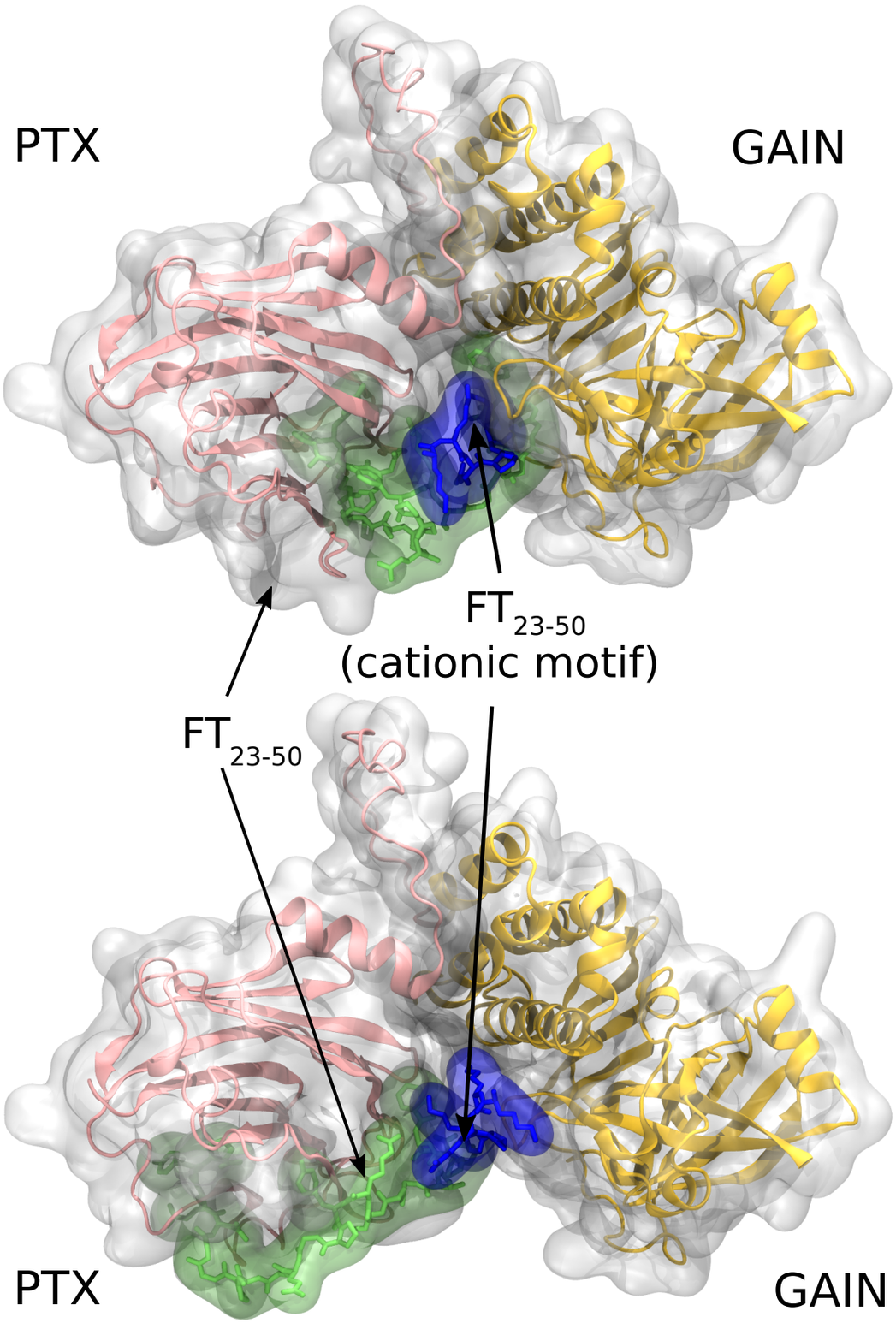
PTX
GAIN
FT23-50
(cationic motif)
FT23-50
PTX
GAIN

B

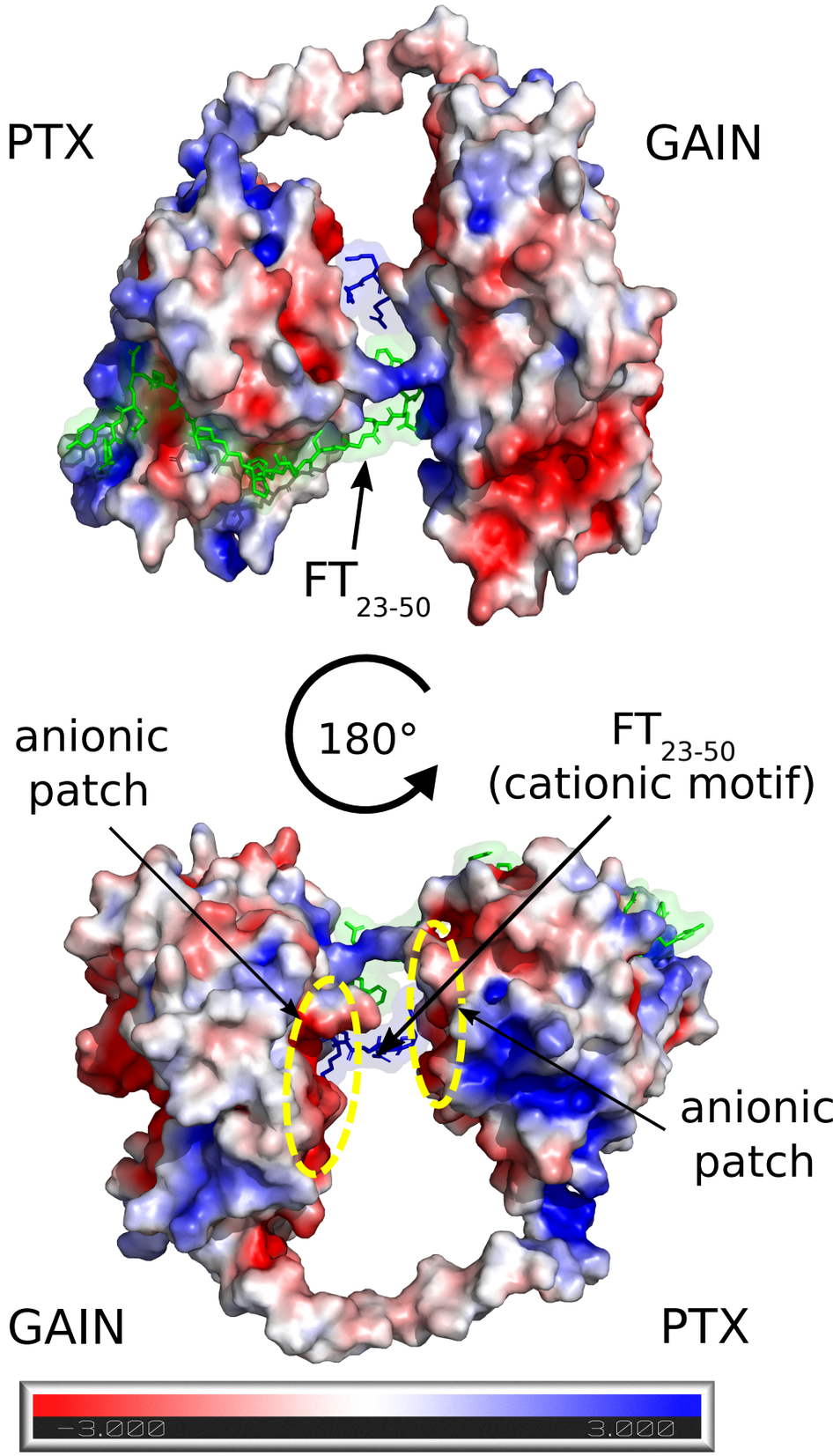
PTX
GAIN
FT23-50
anionic
patch
180°
FT23-50
(cationic motif)
anionic
patch
GAIN
PTX
−3.000
3.000

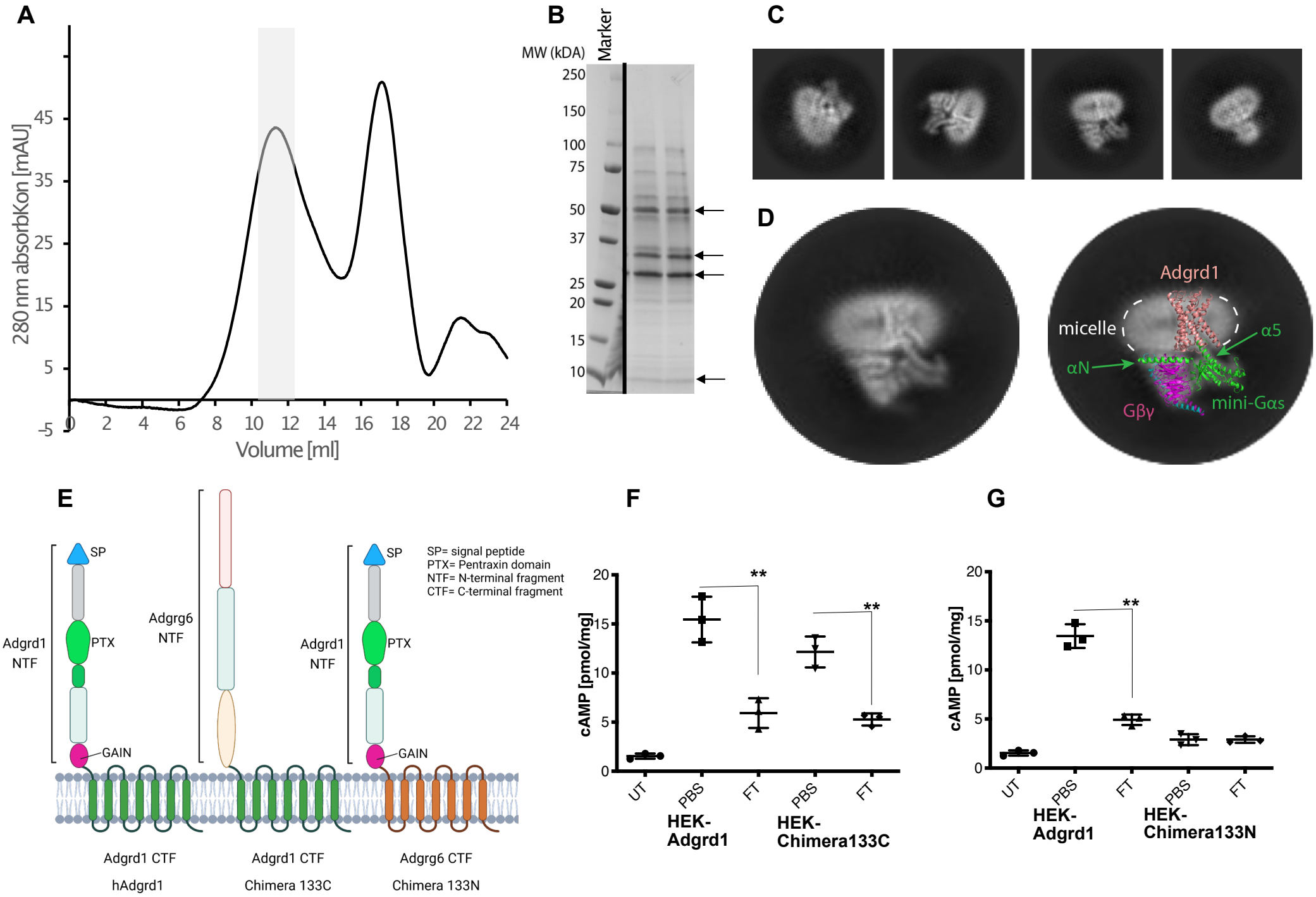
A
280 nm absorbKon [mAU]
45
35
25
15
5
-5
0 2 4 6 8 10 12 14 16 18 20 22 24
Volume [ml]
B
MW (kDA)
Marker
250
150
100
75
50
37
25
20
15
10
C
D
Adgrd1
micelle
α5
αN
Gβγ
mini-Gαs
E
SP
PTX
GAIN
Adgrd1 NTF
Adgrg6 NTF
SP= signal peptide
PTX= Pentraxin domain
NTF= N-terminal fragment
CTF= C-terminal fragment
Adgrd1 CTF
hAdgrd1
Adgrd1 CTF
Chimera 133C
Adgrg6 CTF
Chimera 133N
F
cAMP [pmol/mg]
20
15
10
5
0
**
**
UT
PBS
FT
PBS
FT
HEK-Adgrd1
HEK-Chimera133C
G
cAMP [pmol/mg]
20
15
10
5
0
**
UT
PBS
FT
PBS
FT
HEK-Adgrd1
HEK-Chimera133N

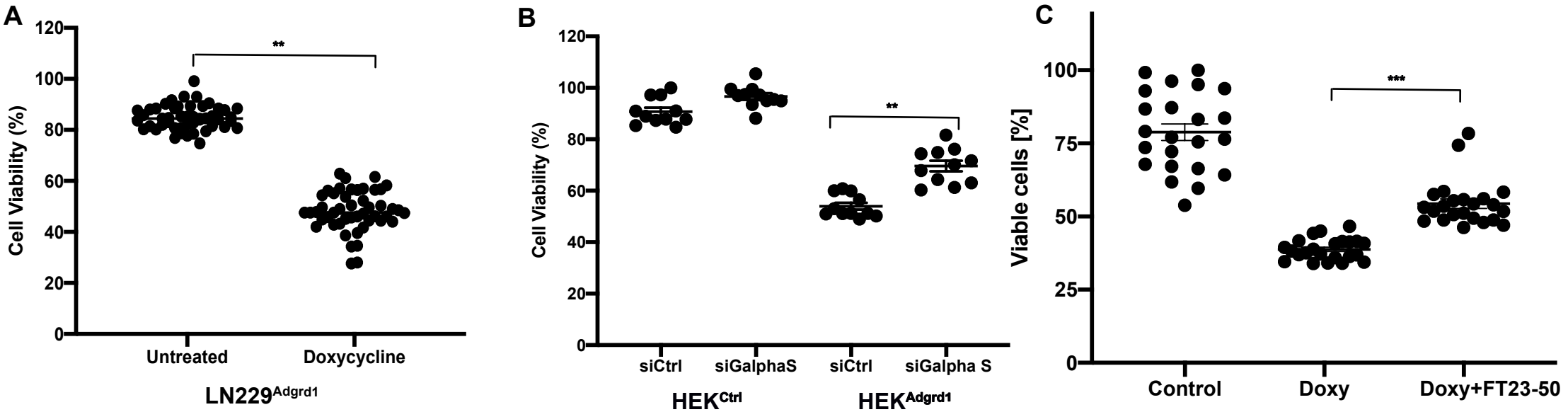
A
Cell Viability (%)
120
100
80
60
40
20
0
**
Untreated
Doxycycline
LN229Adgrd1
B
Cell Viability (%)
120
100
80
60
40
20
0
**
siCtrl
siGalphaS
siCtrl
siGalpha S
HEKCtrl
HEKAdgrd1
C
Viable cells [%]
100
75
50
25
0
***
Control
Doxy
Doxy+FT23-50

Figure 5

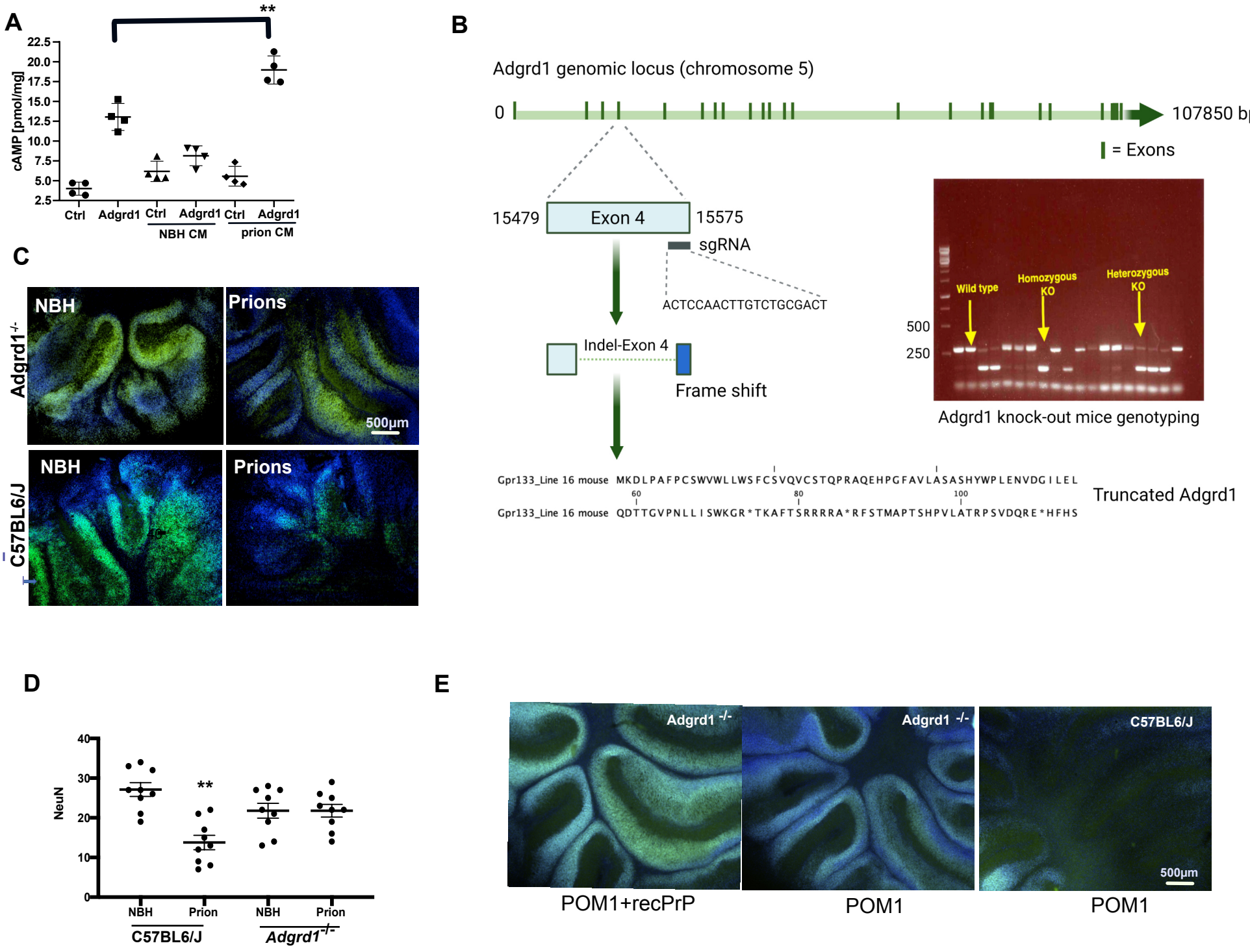
A
**
cAMP [pmol/mg]
22.5
20.0
17.5
15.0
12.5
10.0
7.5
5.0
2.5
Ctrl
Adgrd1
Ctrl
Adgrd1
Ctrl
Adgrd1
NBH CM
prion CM
B
Adgrd1 genomic locus (chromosome 5)
0
107850 bp
= Exons
15479
Exon 4
15575
sgRNA
ACTCCAACTTGTCTGCGACT
Indel-Exon 4
Frame shift
Wild type
Homozygous KO
Heterozygous KO
500
250
Adgrd1 knock-out mice genotyping
Gpr133_Line 16 mouse MKDLPAFPCSWVWLLWSFCSVQVCSTQPRAQEHPGFAVLASASHYWPLENVDGILEL
Gpr133_Line 16 mouse QDTTGVPNLLISWKGR*TKAFTSRRRRA*RFSTMAPTSHPVLATRPSVDQRE*HFHS
Truncated Adgrd1
C
NBH
Prions
Adgrd1-/-
500µm
NBH
Prions
C57BL6/J
D
NeuN
40
30
20
10
0
**
NBH
Prion
NBH
Prion
C57BL6/J
Adgrd1-/-
E
Adgrd1 -/-
Adgrd1 -/-
C57BL6/J
500µm
POM1+recPrP
POM1
POM1

Figure 6

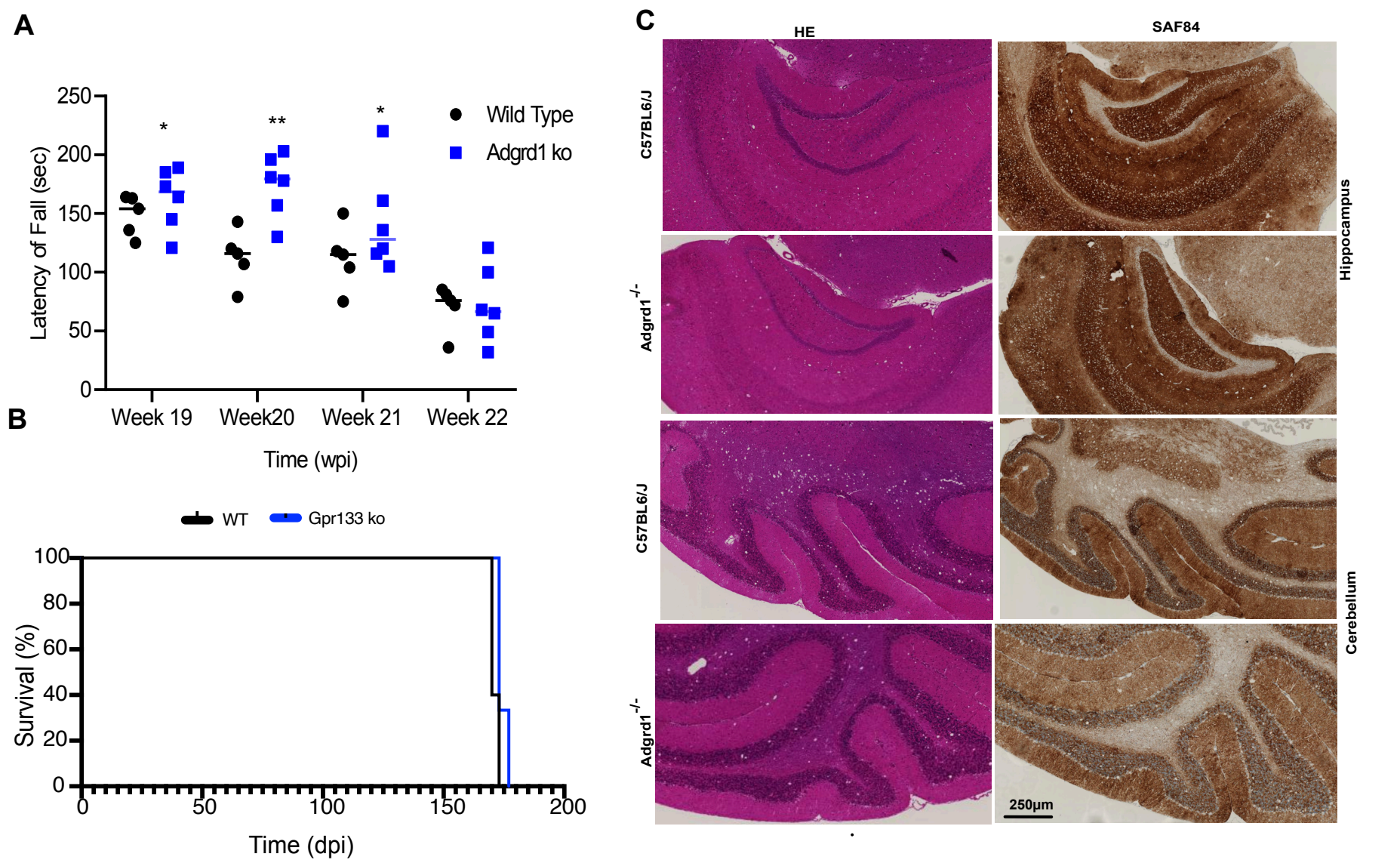
A
Latency of Fall (sec)
250
200
150
100
50
0
*
**
*
Wild Type
Adgrd1 ko
Week 19
Week20
Week 21
Week 22
Time (wpi)
B
WT
Gpr133 ko
Survival (%)
100
80
60
40
20
0
0
50
100
150
200
Time (dpi)
C
HE
SAF84
C57BL6/J
Adgrd1-/-
C57BL6/J
Adgrd1-/-
Hippocampus
Cerebellum
250μm